

Table 6-10 Results of Transition Material Tests (Nam Ngao Dam Site)

(1) River deposits

SAMPLE No.	DEPTH (m)	USCS. SOIL GROUP	C _u	C _c	FM	Gradation Analysis										Dry Density (t/m ³)	Percentage of wear (%)
						-76.2mm	-50.8mm	-25.4mm	-4.76mm	-2.38mm	-1.19mm	-0.59mm	-0.297mm	-0.105mm			
TFNG-1	0.4 - 1.9	GP	120.00	8.53	7.42	73.64	50.76	37.42	21.30	17.50	14.41	11.46	6.40	2.67			
TFNG-2	0.3 - 1.9	GP	71.43	0.90	6.19	95.27	86.06	61.71	35.77	28.75	23.64	18.06	5.70	2.01			
TFNG-3	0.3 - 2.1	GP	75.86	0.16	5.72	96.41	75.18	63.05	43.32	37.64	31.63	25.04	11.55	3.36			
TFNG-4	0.5 - 1.9	GP	78.33	10.25	7.53	77.68	63.94	39.84	16.97	14.24	12.52	10.47	4.48	1.31			
TFNG-1,2,3,4		GP	140.00	1.27	6.72	75.34	68.05	48.99	31.37	26.94	23.39	19.56	9.79	3.76	2.151		
TFNG-5	0.0 - 1.6	GP	130.23	59.97	7.75	82.88	43.00	24.78	16.97	15.91	15.30	13.28	5.73	1.91		28.41	
TFNG-6	0.3 - 2.5	GP	106.00	18.26	7.60	76.85	54.68	33.32	18.31	16.73	15.47	11.33	3.81	1.14			
TFNG-7	0.4 - 2.3	GP	148.57	17.80	7.47	77.89	58.16	36.66	17.92	16.42	15.34	13.27	8.43	3.86			
TFNG-8	0.3 - 1.8	GP-SP	93.33	0.06	4.78	100.00	84.27	69.04	52.01	48.79	45.59	42.40	25.28	11.55			
TFNG-5,6,7,8		GP	142.42	34.11	7.38	84.02	66.68	32.46	17.73	16.47	15.53	14.02	9.92	5.06	2.170		
TFNG-9	0.2 - 1.8	SP	2.17	1.04	2.16	—	100.00	97.96	91.64	82.12	75.15	71.02	56.36	16.06			
TFNG-10	0.2 - 1.5	GM	152.78	2.13	7.14	73.92	56.74	44.20	26.45	20.57	16.52	13.64	8.67	3.46			
TFNG-9,10		GP	311.11	0.10	6.34	66.47	62.91	50.37	37.73	33.13	29.64	27.41	20.98	6.85	1.856		
TFNG-11	0.1 - 1.2	GP	82.76	24.28	7.63	78.00	63.55	30.09	18.55	16.62	14.31	11.15	4.54	1.08			
TFNG-11,12		GP	66.67	0.31	6.05	90.12	79.33	62.45	39.20	34.20	29.41	20.73	6.65	1.39	2.105		
TFNG-13	0.1 - 1.4	GP	62.22	21.61	7.94	76.75	42.88	25.67	16.16	14.69	12.31	7.71	1.95	0.49			
TFNG-14	0.2 - 1.6	GP	36.67	7.58	7.45	100.00	69.77	39.60	14.13	11.16	10.14	8.86	4.25	1.51			
TFNG-15	0.1 - 1.4	GP	52.44	3.43	7.11	100.00	72.91	45.22	21.12	17.01	12.71	9.33	4.32	1.20			
TFNG-14,15		GM	80.00	2.72	6.69	87.28	76.47	56.13	28.25	23.31	18.55	14.67	7.04	2.43	2.205		
TFNG-16	0.2 - 1.8	GM	14.00	2.24	8.28	64.73	46.71	29.11	9.75	6.99	5.71	4.96	2.82	1.02			
TFNG-17	1.0 - 2.0	GM	352.94	1.98	7.39	46.00	38.93	34.08	29.52	28.87	27.70	20.01	6.76	1.41			
TFNG-16,17		GP	167.39	7.23	7.77	49.73	45.24	37.30	20.51	17.78	16.18	12.73	5.31	1.43	2.155		

(2) Terrace deposits

SAMPLE No.	DEPTH (m)	USCS. SOIL GROUP	SP.GR.	C _u	C _c	FM	Gradation Analysis										COMPACTION	
							-19.1mm	-4.76mm	-2.38mm	-1.19mm	-0.297mm	-0.105mm	-0.074mm	Max. r _D (t/m ³)	Wopt. (%)			
TRNG-1	0.4 - 3.4	ML	2.59				—	94.51	90.03	89.75	86.36	71.30	51.59					
TRNG-1	3.4 - 4.3	GP	2.54	168.0	30.86	6.91	31.67	22.27	19.49	17.51	11.64	7.42	5.23					
TRNG-2	0.3 - 4.8	GM	2.55				62.17	54.42	52.51	51.33	46.38	31.41	22.49					
TRNG-3	0.3 - 4.3	ML	2.57				—	100.00	99.97	98.76	85.37	67.65	53.47					
TRNG-4	0.3 - 3.1	SM	2.57				72.67	70.33	69.11	68.20	62.40	41.27	26.92					
TRNG-5	0.3 - 3.3	SM	2.56				68.08	60.07	56.40	49.42	32.90	21.93	15.31					
TRNG-6	0.3 - 2.7	SM	2.58				100.00	95.82	94.68	93.43	81.83	39.53	22.30					
TRNG-6	2.7 - 4.1	GM	2.61				48.53	39.82	37.84	36.35	31.42	21.35	15.67					
TRNG-7	0.4 - 4.1	SM	2.58				95.41	87.27	82.53	78.76	76.52	56.71	42.70					
TRNG-1,2	—	SM	—				76.75	71.40	70.26	69.12	60.68	42.03	33.63	1.838	13.3			
TRNG-3,4	—	SM	—				88.34	85.18	78.54	75.48	73.98	54.46	39.19	1.783	13.8			
TRNG-5,6,7	—	SM	—				83.23	76.66	73.15	69.28	58.05	35.60	26.19	1.812	13.1			

Table 6-11 Results of Soil Tests (Mae Lama Luang Dam Site)

	Sample No.	Depth (m)	Classification of Soils by Unified System	Specific Gravity	Natural Water Content (%)	Atterberg Limits		Gradation Analysis							Compaction & Permeability				Triaxial Compression strength			
						LL (%)	PI (%)	-19.0	-4.76	-2.0	-0.42	-0.074	-0.01	-0.002	Maximum Dry Density (t/m ³)	Optimum Water Content (%)	Coefficient of Permeability (cm/see)	Molded Water Content (%)	Total Stress		Effective Stress	
								mm (%)	mm (%)	mm (%)	mm (%)	mm (%)	mm (%)	mm (%)					ν (Kgf/cm ²)	φ (deg)	ν (Kgf/cm ²)	φ (deg)
A	LY-1	0.1-1.7		2.71	9.1	31.45	6.35	54.8	42.4	37.4	32.0	24.9	17.6	5.0	1.735	15.2	3.0x10 ⁻⁷ (3.5x10 ⁻⁷)	17.0 1)	0.1	16.5	3.0	31.5
	LY-2	0.2-0.4	CM	2.65	8.5	27.00	5.03	82.7	67.2	61.4	56.1	45.5	27.2	12.5	1.830	13.4						
	LY-3	0.2-2.4	CM	2.62	5.0	NP	NP	63.0	48.8	44.6	40.3	27.5	16.7	8.5	1.810	14.65						
	LY-4	0.1-4.2	CM	2.69	6.1	35.55	10.86	77.6	70.2	65.7	60.7	48.4	31.9	19.6	1.835	14.5						
	LY-5	0.1-2.3	CM	2.66	6.4	NP	NP	57.7	45.3	40.3	35.6	24.6	15.1	8.1	1.849	11.9						
	LY-1, 2, 3, 4, 5	—	CM	2.69	6.6	30.10	7.14	89.8	72.6	65.9	60.4	48.8	28.5	13.0	1.820	14.0						
	LY-15	0.3-1.2	CM	2.70	3.1	36.50	8.53	71.4	58.1	49.7	45.4	39.1	28.7	13.5	1.836	14.0						
	"	1.2-5.7	CM	2.73	5.9	28.00	1.84	49.0	27.0	21.7	16.9	12.1	7.5	2.3	1.7614	16.1						
	"	0.3-5.7	SM	2.73	4.7	32.25	5.80	86.3	69.5	59.0	52.3	44.0	31.5	16.0	1.807	15.7						
	LY-16	0.2-2.5	CM	2.66	7.1	26.60	3.89	83.1	72.9	65.4	59.1	44.2	25.0	12.1	1.842	12.8						
"	2.5-4.5	CM	2.66	5.1	NP	NP	57.8	43.0	33.0	21.6	13.4	6.5	2.3	1.868	12.4							
"	0.2-4.5	CM	2.68	5.9	NP	NP	76.6	59.8	50.4	42.3	30.1	16.9	7.5	1.856	12.3	8.9x10 ⁻⁷	14.6					
	Trench R	0.3-1.5	SM	2.72	7.7	28.70	3.55	90.9	70.4	58.3	47.1	37.1	26.2	7.5	1.776	14.3	7.0x10 ⁻⁷	16.4				
B	LY-6	0.3-5.9	CM	2.65	6.3	NP	NP	79.1	55.6	45.1	35.5	23.2	14.6	9.5	1.920	11.6	1.5x10 ⁻⁷ 2)		0	17.5	0	35.0
	LY-7	0.4-4.5	CM	2.68	4.2	NP	NP	76.4	65.0	62.2	59.6	42.4	17.5	7.2	1.586	15.2						
	LY-8	0.4-5.1	ML	2.64	8.9	35.80	4.11	95.0	84.9	83.3	81.8	66.0	27.5	13.0	1.645	18.6						
	LY-9	0.3-5.9	ML	2.65	11.8	32.00	5.73	89.9	86.9	85.6	84.2	64.1	33.1	15.1	1.700	18.1						
	LY-10	0.3-6.6	ML	2.67	16.8	43.30	11.19	96.5	85.1	81.5	79.0	71.2	44.9	28.5	1.678	17.7						
	LY-6, 7, 8, 9, 10	—	ML	2.66	13.0	33.80	5.78	88.4	77.9	74.3	71.0	58.1	32.8	19.9	1.725	16.8	(1.4x10 ⁻⁸)	19.2				
C	LY-17	0.3-3.9	ML	2.67	7.1	41.80	4.72	100.0	97.8	96.5	94.6	82.5	51.9	27.1	1.640	21.7	3.0x10 ⁻⁷					
	"	3.9-5.5	CM	2.70	7.5	44.20	5.24	77.9	63.3	57.3	52.7	46.6	28.4	11.0	1.627	19.4						
	"	0.3-5.5	ML	2.68	8.2	41.60	5.63	88.1	81.7	78.8	76.8	68.2	40.4	20.0	1.630	19.7						
	LY-18	0.2-2.0	MH	2.67	19.6	54.70	17.06	87.6	72.7	68.5	67.3	63.2	43.0	29.3	1.645	20.5						
	LY-19	0.2-2.4	MH	2.68	9.3	58.85	17.16	100.0	96.8	96.1	95.2	89.5	58.0	36.8	1.520	23.6						
	"	2.4-5.8	ML	2.69	7.7	43.00	5.02	89.5	83.6	81.7	80.8	70.6	25.1	7.5	1.544	20.0						
	"	0.2-5.8	ML	2.70	6.2	43.90	4.92	98.4	92.9	91.6	90.8	84.2	44.9	26.1	1.531	23.1						
	LY-17, 18, 19	—	ML	2.66	7.8	43.80	8.51	92.3	85.3	83.0	81.4	73.8	44.0	25.0	1.601	20.2	24.6					
Left bank of dam	LY-11	0.2-3.0	CM	2.64	4.3	25.40	2.69	85.6	66.2	55.7	46.5	34.1	22.5	10.0	1.846	13.0	5.0x10 ⁻⁷					
	"	3.0-6.0	CM	2.67	7.5	23.55	2.42	79.0	53.1	42.2	33.3	23.1	12.0	5.0	1.830	14.4						
	"	0.2-6.0	CC-CM	2.67	0.4	25.40	5.97	82.9	55.1	45.6	37.7	27.7	18.2	8.1	1.845	14.3						
	LY-12	0.4-3.0	CM	2.71	10.4	28.40	4.96	72.6	66.6	64.0	60.2	46.1	22.5	14.8	1.781	14.7						
	LY-13	0.3-3.0	ML	2.74	12.4	31.08	6.26	97.0	86.2	80.8	75.4	64.0	43.1	13.2	1.737	16.9						
	"	3.0-6.0	CM	2.76	9.5	NP	NP	27.6	20.5	18.3	15.8	12.1	7.5	2.0	1.700	17.0						
	"	0.3-6.0	CM	2.76	9.5	NP	NP	65.2	52.8	48.7	44.2	36.6	23.5	7.56	1.745	15.2						
	LY-14	0.1-1.0	CM	2.65	6.4	37.80	9.45	77.2	61.2	51.9	44.4	38.2	28.6	15.1	1.820	15.2						
	LY-11, 12, 13	—	CM	2.65	2.6	28.90	4.37	86.3	71.9	65.2	58.4	46.4	30.2	12.4	1.751	15.0						
	Drill Hole SP-1	1.0-2.0	ML	2.74	-	26.00	2.39	97.4	87.1	79.6	67.7	52.1	33.4	10.0								
"	11.0-12.0	SM	2.79	-	NP	NP	100.0	95.5	86.5	67.0	49.3	32.2	7.1									
Trench L	0.3-2.5	ML	2.67	5.0	31.40	4.82	90.3	78.6	73.4	68.8	58.3	39.4	13.5	1.753	18.3	19.5						

Remarks : 1) The name of Borrow Area

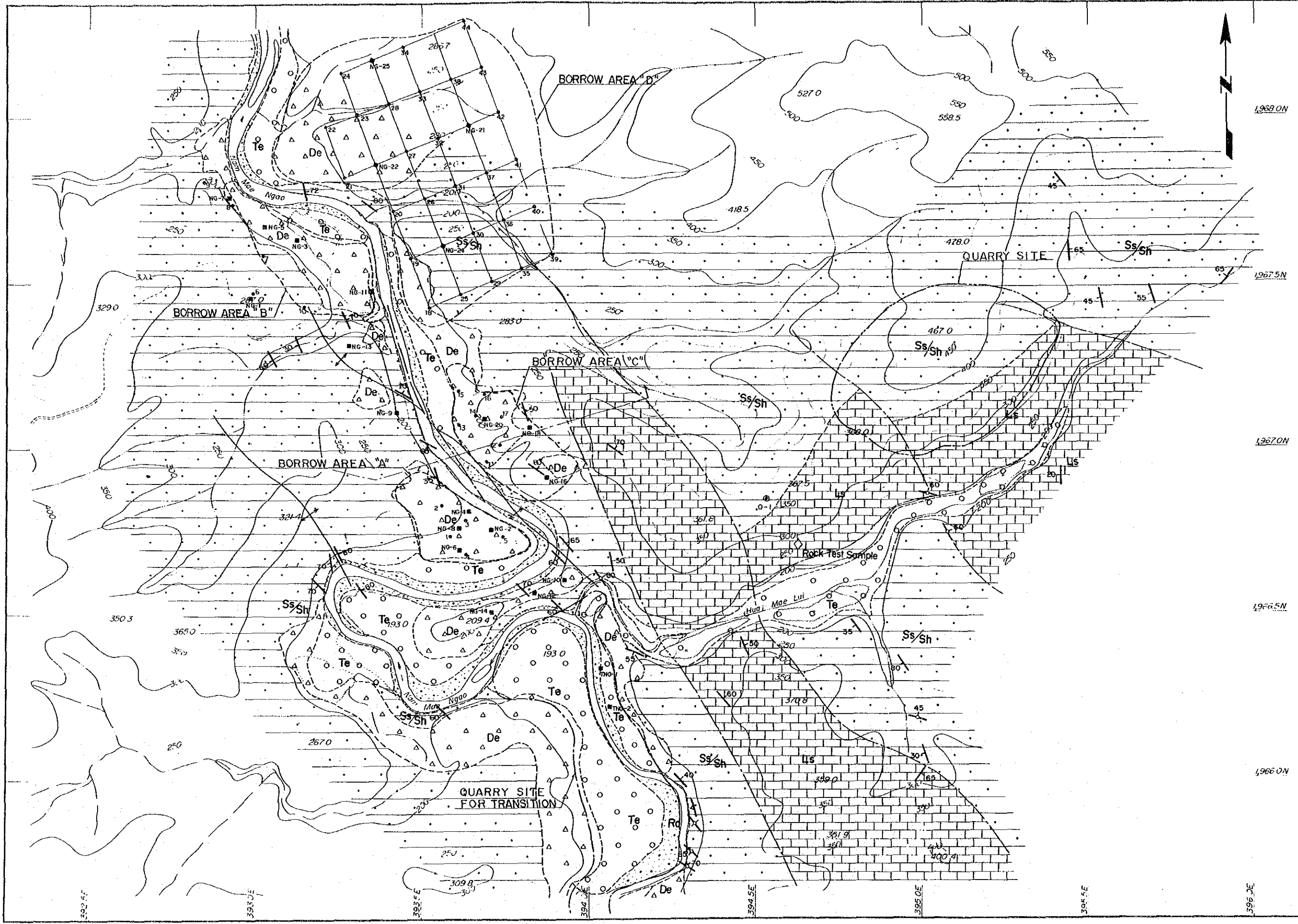
2) Coefficient of Permeability at optimum water content 2

Table 6-12 Results of Filter Material Tests (Mae Lama Luang)

Sample No.	Depth (m)	Usqs. Soil Group	Max. Dry Density (t/m ³)	C _u	C _c	FM	Gradation Analysis											Percentage of Wear (%)
							-75 mm	-38.1 mm	-19.1 mm	-9.52 mm	-4.76 mm	-2.0 mm	-0.84 mm	-0.42 mm	-0.105 mm			
TFLY-1	0.0 - 1.50	SP	↑	3.75	1.20	3.85	100.0	95.27	94.68	89.28	84.50	71.80	30.75	10.83	2.24			
TFLY-2	0.0 - 0.70	SP	2.133	1.91	1.25	2.51		100.0	95.93	92.27	90.34	86.89	81.46	63.36	3.22			
TFLY-3	0.0 - 3.10	GP	↓	55.77	0.15	6.18	100.0	65.00	53.94	44.32	39.38	34.44	23.15	7.24	0.74			
TFLY-4	0.0 - 2.10	GP	↓	35.56	0.70	6.86	86.30	59.41	52.69	39.37	30.58	21.17	9.59	2.72	0.48			
TFLY-5	0.0 - 0.80	GP	2.192	48.75	4.62	7.21	91.84	59.40	37.39	28.60	22.23	17.17	10.96	5.30	1.19			
TFLY-6	0.0 - 1.80	GP	↑	39.29	0.36	6.30	100.0	78.26	57.16	42.10	34.92	26.03	14.34	8.30	0.88			
TFLY-7	0.0 - 1.80	GP	2.219	32.05	0.63	6.63	83.50	66.63	60.11	40.64	34.03	23.43	10.85	5.76	1.09			
TFLY-8	0.0 - 0.55	GW	↑	66.67	2.19	6.70	90.74	65.72	45.10	34.78	28.14	19.45	13.10	9.30	1.53			
TFLY-9	0.0 - 2.10	GP	↑	48.65	6.34	7.19	84.50	63.98	38.24	26.18	21.73	18.07	12.00	5.69	2.08	Grade "A" = 27.09		
TFLY-10	0.0 - 1.65	GP	2.186	27.69	7.71	7.35	100.0	60.43	30.53	19.74	15.58	12.19	8.14	5.65	3.96			
TFLY-11	0.0 - 1.75	GP	↑	100.0	6.72	7.28	89.91	50.98	35.23	26.57	21.56	17.71	13.75	7.58	2.05	Grade "E" = 20.47		
TFLY-12	0.0 - 1.75	GP	↑	119.57	11.42	7.27	90.92	48.17	33.20	24.73	20.75	18.33	14.65	8.75	3.02			
TFLY-13	0.0 - 0.95	SP-SM	↑	17.33	0.33	4.51	100.0	69.69	65.00	63.69	62.36	58.76	44.98	33.51	13.10			
TFLY-14	0.0 - 2.00	GW	↑	24.67	2.13	7.22	93.50	64.28	42.17	29.20	21.01	12.60	5.74	2.53	1.13			
TFLY-15	0.0 - 1.90	GW	2.244	53.33	2.09	7.18	88.64	55.93	43.12	30.36	22.75	14.94	9.60	6.54	1.45			
TFLY-16	0.0 - 1.00	GP	↑	31.67	0.22	5.99	100.0	80.05	58.24	47.41	40.10	33.55	16.94	4.59	0.47			
TFLY-17	0.0 - 1.80	GP	↑	56.92	0.63	6.70	89.41	61.94	50.05	39.46	32.23	25.08	13.80	4.69	1.13			
TFLY-18	0.0 - 0.70	SP	↑	3.37	0.79	2.91		100.0	98.61	92.67	83.05	59.78	27.09	2.82				
TFLY-19	0.0 - 1.75	GP	↑	76.68	8.90	5.76	100.0	70.12	54.81	49.14	45.27	39.39	26.99	12.16	2.11			
TFLY-20	0.0 - 0.95	GW	2.223	58.95	2.71	7.51	73.00	52.75	37.36	27.34	21.59	16.50	8.79	3.46	1.06			
TFLY-21	0.0 - 1.50	GP	↑	77.61	0.51	7.05	80.18	50.19	41.46	34.96	30.33	24.16	13.20	4.41	1.55			
TFLY-22	0.0 - 2.40	GP	2.305	59.42	9.05	7.45	78.11	54.55	32.82	25.78	19.18	14.23	11.25	7.61	1.55			
TFLY-23	0.0 - 0.80	GP	2.305	79.31	5.40	7.34	78.42	53.59	40.29	27.09	20.31	14.85	12.44	9.07	1.88			
TFLY-24	0.0 - 1.20	GW	2.266	361.11	2.05	6.64	83.29	49.90	40.93	33.35	29.91	27.32	24.19	19.25	7.76			
TFLY-25	0.0 - 1.20	GP	↑	106.82	0.21	6.67	85.00	55.77	42.23	38.09	35.13	30.39	18.92	8.89	0.78			
TFLY-26	0.0 - 1.55	GW	2.266	45.83	1.32	6.91	87.46	63.22	45.92	36.01	27.85	21.19	11.04	4.34	1.59			
TFLY-27	0.0 - 1.90	GP	↑	96.87	0.61	7.14	82.43	49.54	40.96	33.46	29.75	24.87	14.15	5.31	1.43			
TFLY-28	0.0 - 0.45	GW	↑	40.82	2.45	7.27	79.14	59.30	41.68	29.61	23.59	18.01	8.34	4.12	2.28	Grade "A" = 27.09		
TFLY-29	0.0 - 1.30	GW	2.219	25.33	1.72	7.33	84.63	61.42	43.34	29.01	20.67	13.72	8.55	3.79	0.67			
TFLY-30	0.0 - 0.45	GP	↑	37.50	0.38	6.59	100.0	69.28	47.68	38.40	32.72	26.88	14.53	4.26	0.76	Grade "E" = 20.47		
TFLY-31	0.0 - 1.55	GP	2.190	78.26	7.57	6.04	100.0	87.60	65.10	40.98	33.29	21.99	20.01	17.50	2.87			
TFLY-32	0.0 - 0.75	GP	2.190	40.98	0.24	6.55	71.50	66.44	66.21	44.10	37.14	30.81	15.29	5.83	1.51			
TFLY-33	0.0 - 1.00	GW	2.218	101.82	1.33	6.93	61.50	53.19	40.61	31.79	26.37	18.89	12.63	7.59	1.53			
TFLY-34	0.0 - 1.05	GP	2.218	67.27	0.41	6.64	86.50	58.97	46.50	40.79	34.58	26.30	14.08	7.77	4.87			

Table 6-13 Results of Rock Material Tests (Mae Lama Luang)

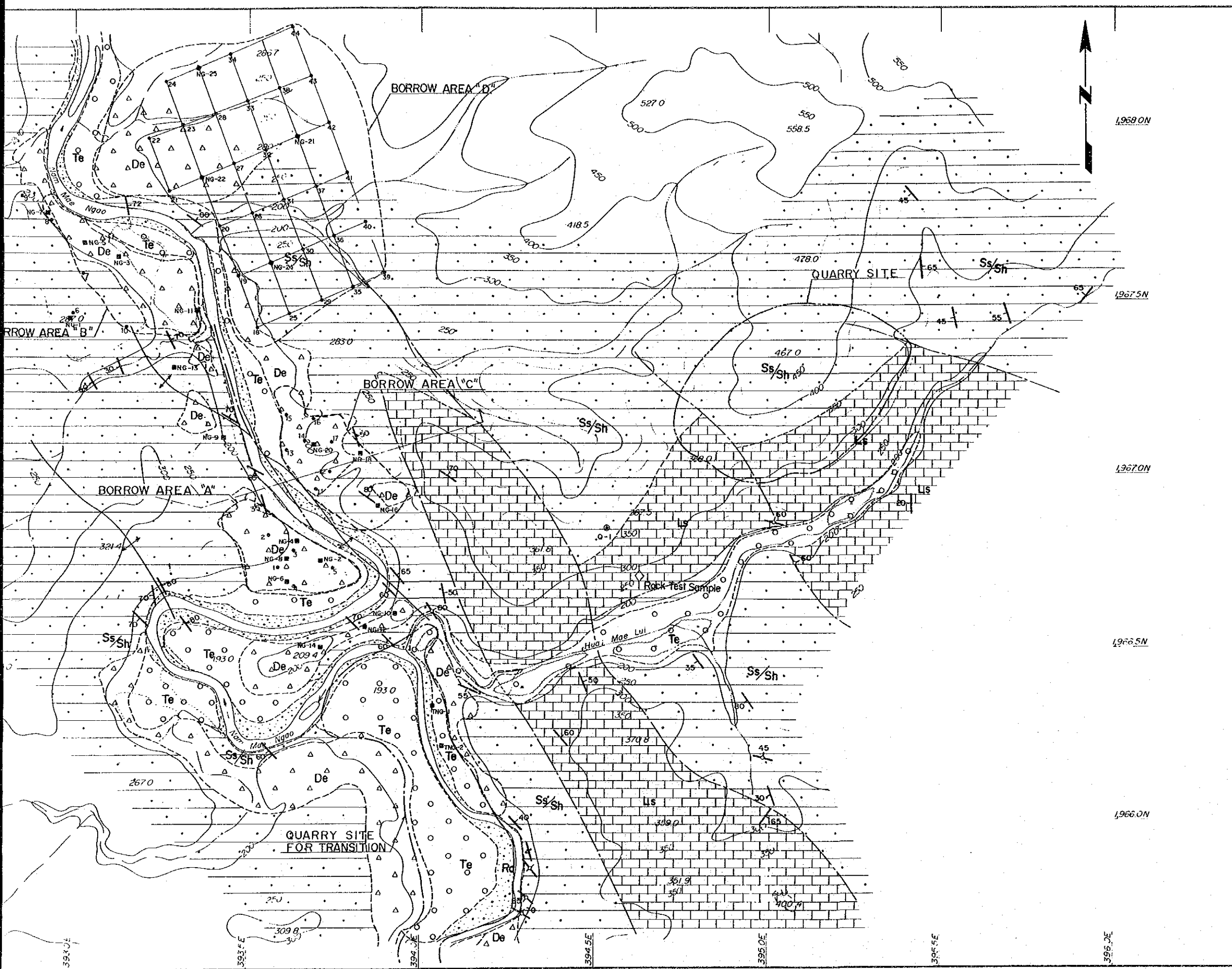
Categories	Unit	Quarry Site "A"		Quarry Site "B"	
		R-1	R-2	Q-1	Q-2
Los Angeles abrasion test					
Percentage of wear grade "A"	%	24.07	24.64	20.57	24.62
Percentage of wear grade "E"	%	34.90	32.33	16.27	18.63
Crushing value	%	24.16	23.00	15.82	19.08
Wt. loss in soundness test	%	0.12	0.22	0.34	0.23
Specific gravity (Sat. surface-dry)	—	2.70	2.71	2.64	2.72
Water absorption	%	0.43	0.48	0.64	0.73
Elongation index (BS : 812)	—	0.60	0.43	0.73	0.81
Flakiness index (BS : 812)	—	0.37	0.33	0.26	0.47



- △ De
- Rd
- Te
- ▭ Ls
- ▨ Ss/Sh

- 70
- 70
-
-
-
- NG-7
-
- ◇

NAM YI
HYDROE
CONS
NAI
BOF
Fig 6-1

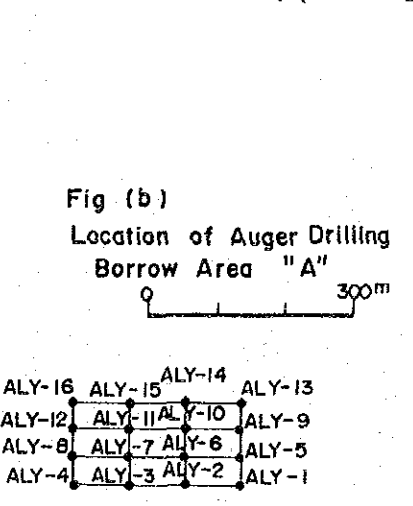
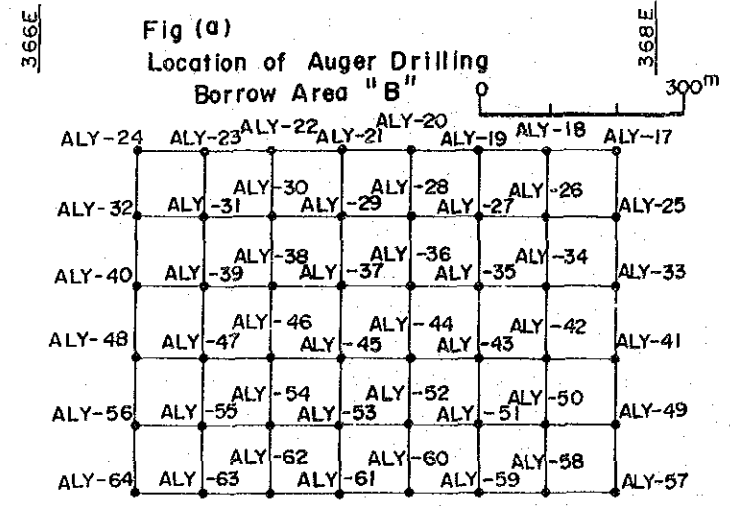
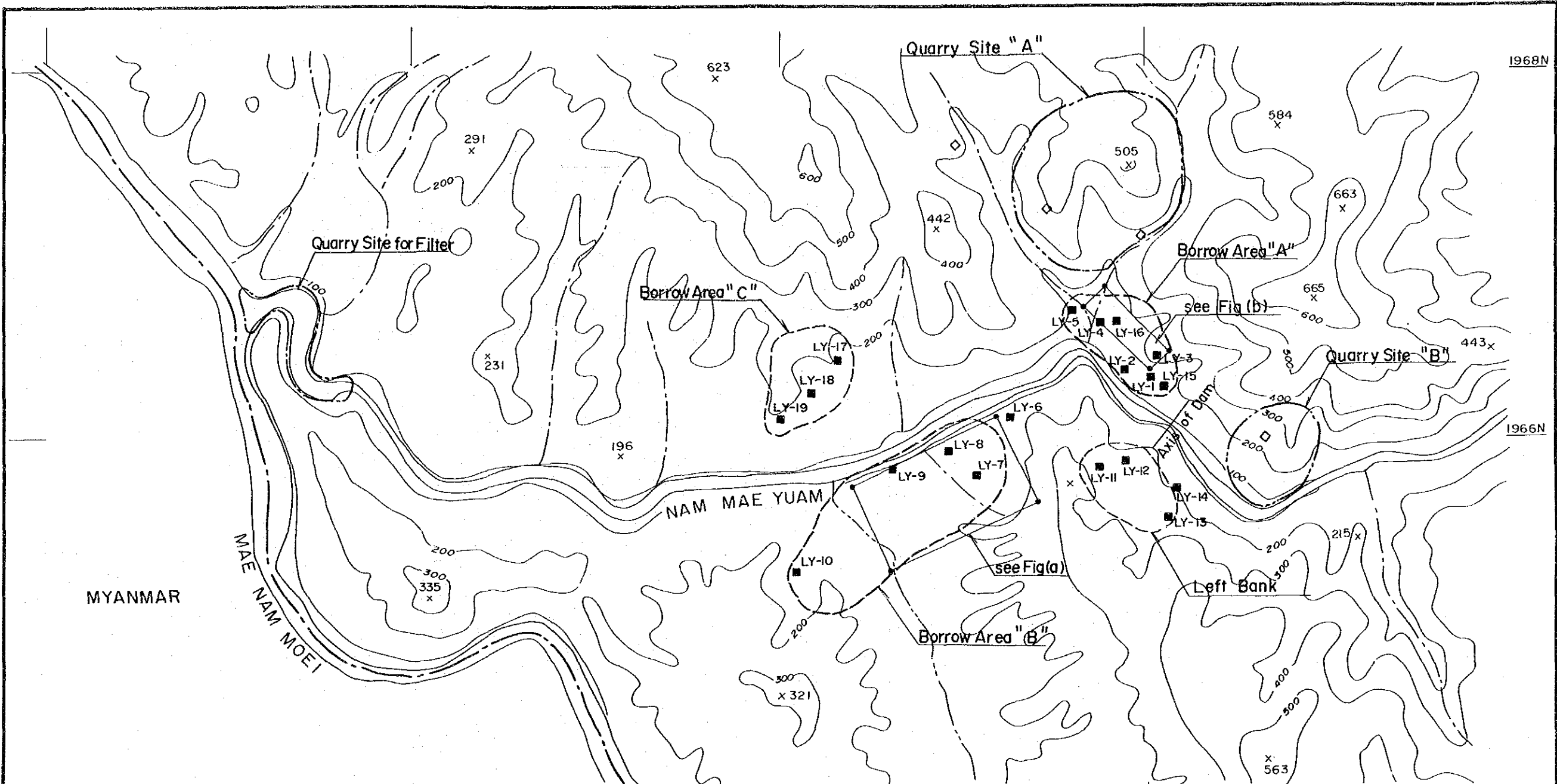


- LEGEND**
- Detritus, Topsoil, Thick residual soil and Rock fragment
 - River deposit
 - Terrace deposit
 - Limestone
 - Alternation of sandstone and shale
 - Strike and dip of strata
 - Strike and dip of fault
 - Geologic boundary
 - Fault
 - Borrow Area
 - Quarry Site for Transition Material
 - Quarry Site
 - Test Pit (NG: for Imperiums Core Material)
(TNG: for Transition or Filter Material)
 - Auger Drilling
 - Locality for rock test sample

0 500m

**NAM YUAM RIVER BASIN INTEGRATED
 HYDROELECTRIC DEVELOPMENT PROJECT**
CONSTRUCTION MATERIAL
NAM NGAO DAM SITE
BORROW AREA and QUARRY SITE

Fig 6-10



LEGEND

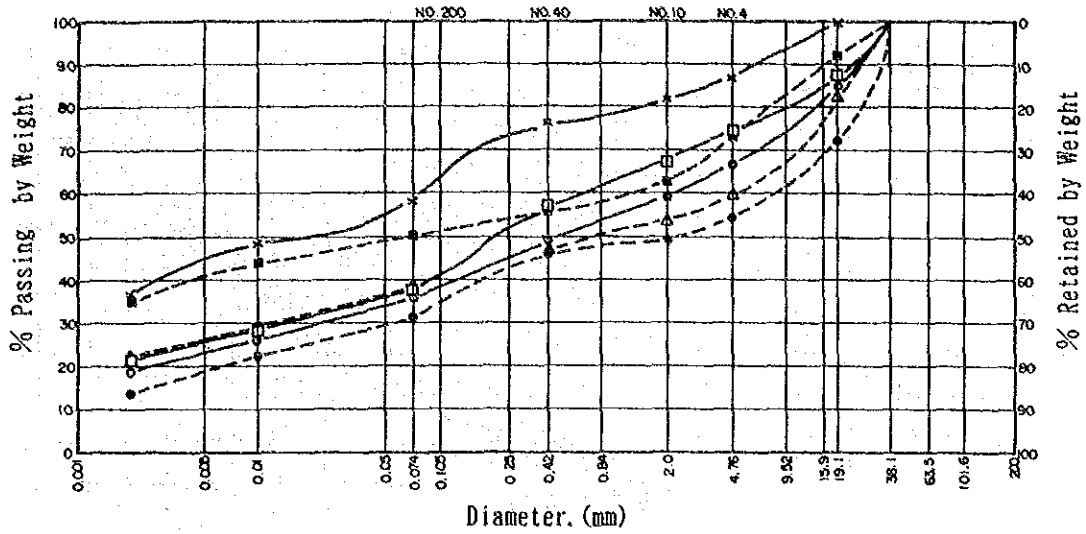
- Borrow Area
- Quarry Site for Filter Material
- Quarry Site
- Test Pit
- Auger Drilling
- Locality for rock test samples

0 1 km

NAM YUAM RIVER BASIN INTEGRATED HYDROELECTRIC DEVELOPMENT PROJECT
CONSTRUCTION MATERIAL
MAE LAMA LUANG DAM SITE
BORROW AREA and QUARRY SITE

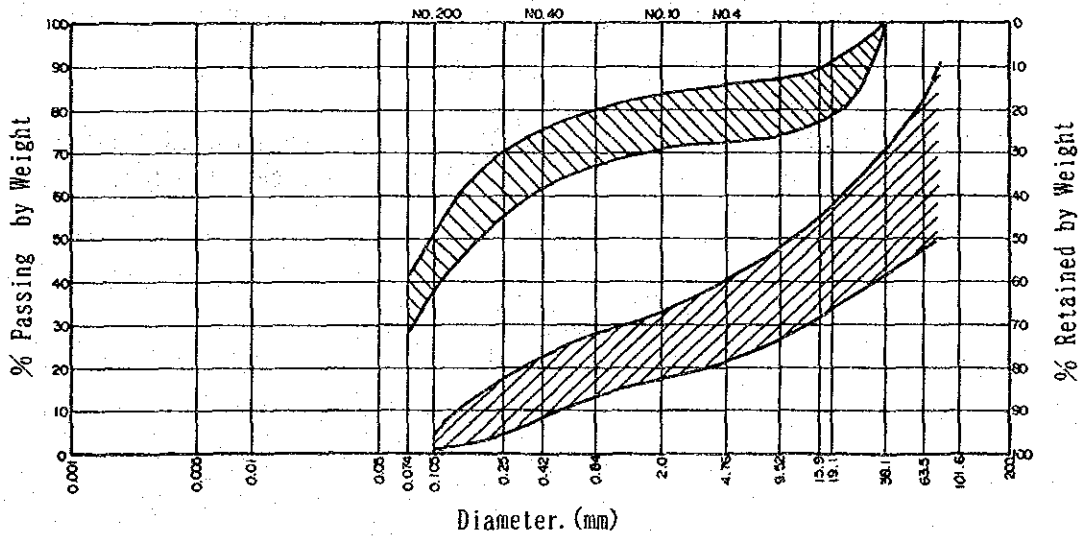
Fig 6 - 11

(a) Impervious Core Materials



No.	SAMPLE NUMBER	DEPTH (m)	SYMBOL	SOIL CLASSIFICATION	SPECIFIC GRAVITY	WATER CONTENT	ATTERBERG LIMITS		
							LL	PL	PI
1	Area "A" NG-2, 4, 6, 8	0.4 ~ 6.5m mixed	—○—	SM	2.70	13.8	47.7	29.9	17.8
2	Area "A" NG-10, 12, 14	0.5 ~ 6.3m mixed	—●—	CM	2.70	6.6	30.5	23.3	7.2
3	Area "B" NG-1, 3, 5, 7	0.3 ~ 4.9m mixed	—□—	SM	2.69	7.7	44.3	28.8	15.5
4	Area "B" NG-9, 11, 13	0.4 ~ 3.3m mixed	—■—	MH	2.71	18.0	57.7	32.2	25.5
5	Area "C" NG-16, 18, 20	0.4 ~ 7.0m mixed	—△—	GM	2.68	—	35.5	24.9	10.6
6	Area "D" NG-21, 22, 24, 25	0.2 ~ 3.8m mixed	—×—	ML	2.74	9.9	40.8	26.2	14.6

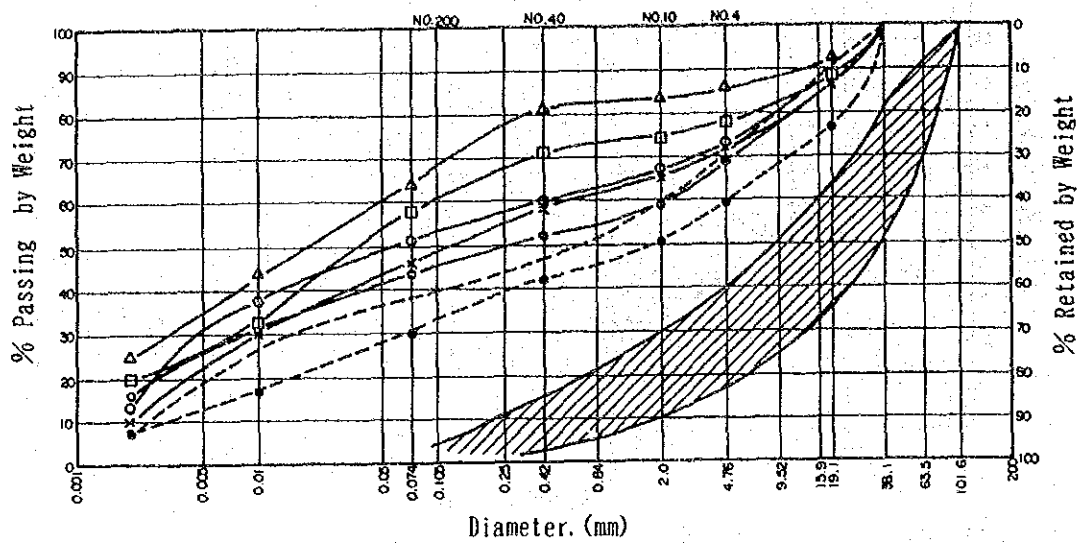
(b) River deposits and Terrace deposits



Legend

- ▨ River deposits TFNG - 1 ~ 17, 0.0 ~ 2.0m
- ▩ Terrace deposits TRNG - 1 ~ 7, 0.3 ~ 4.8m

Fig. 6 - 12 Particle Size Distribution of Impervious Core and Transition Materials (Nam Ngao Dam Site)



No.	SAMPLE NUMBER	DEPTH (m)	SYMBOL	SOIL CLASSIFICATION	SPECIFIC GRAVITY	WATER CONTENT	ATTERBERG LIMITS			
							LL	PL	PI	
Impervious Core Materials	1	Area "A" LY-1~5	0.1~4.7m mixed	—○—	CM	2.69	6.6	30.1	23.0	7.1
	2	Area "A" LY-15	0.3~5.7	—○—	CM	2.73	4.7	32.3	26.5	5.8
	3	Area "A" LY-16	0.2~4.5	—●—	CM	2.68	5.9	—	NP	—
	4	Area "A" Trench R	0.3~1.5	—x—	SM	2.72	7.7	28.7	25.1	3.6
	5	Area "B" LY-6~10	0.3~6.6m mixed	—□—	ML	2.66	13.0	33.8	28.0	5.8
	6	Area "C" LY-17~19	0.3~5.8m mixed	—△—	ML	2.66	7.8	43.8	35.3	8.5
	7	Left Bank LY-11~13	0.2~6.0m mixed	—x—	CM	2.65	2.6	28.9	24.5	4.4
Filter Materials	TFLY-1~35 (except TFLY-1·2)	0.0~3.10 ·13·18·25·32)	///	GP·GW	—	—	—	—	—	

Fig. 6-13 Particle Size Distribution of Impervious Core and Filter Materials (Mae Lama Luang Dam Site)

CHAPTER 7

SEISMICITY

CHAPTER 7 SEISMICITY

CONTENTS

	<u>Page</u>
7.1 General	7 - 1
7.2 Structural Geology	7 - 1
7.2.1 Geological Outline	7 - 1
7.2.2 Structural Geology of Thailand	7 - 3
7.2.3 Major Faults in Thailand	7 - 6
7.2.4 Moei-Uthai Thani Fault	7 - 7
7.3 Seismicity of Thailand	7 - 11
7.3.1 Tectonic Plates and Seismicity	7 - 11
7.3.2 Regional Stress Field around Thailand	7 - 12
7.3.3 Seismicity in and around Thailand	7 - 13
7.3.4 Seismic Activity around the Project Site	7 - 13
7.3.5 Seismic Events in 1983	7 - 17
7.4 Seismic Risk Analysis	7 - 37
7.4.1 Estimation of Maximum Acceleration	7 - 37
7.4.2 Seismic Risk Map for Thailand	7 - 41
7.5 Seismic Coefficient for the Project Site	7 - 53

List of Tables

- Table 7-1 Major Historical Earthquakes in and near Thailand
- Table 7-2 List of Selected Earthquakes for Fault Plane Solutions
- Table 7-3 Representative Reservoir Induced Earthquakes
- Table 7-4 Number of Earthquakes in a Year during the Period from 1901 to 1987
- Table 7-5 Distribution of Magnitude and Epicentral Distance of the Seismicity Data
- Table 7-6 Maximum Annual Acceleration during a Year from 1959 to 1987
- Table 7-7 Maximum Acceleration expected at the Project Site for Four Return Periods (gal)
- Table 7-8 Estimates of Maximum Acceleration at Nam Yuam Project Area
- Table 7-9 Estimated Value of Design Seismic Coefficient based on the Maximum Accelerations

List of Figures

- Fig. 7-1 General Geological Structure of Southeast Asia
- Fig. 7-2 Schematic Structural Map of Thailand and Surrounding Regions
- Fig. 7-3 Major Faults in the North-Western Part of Thailand
- Fig. 7-4 Distribution of Major Tectonic Plates on the Earth and Plate Boundaries
- Fig. 7-5 Epicenters of Earthquakes of Magnitude : $M \geq 4$ and Focal Depth : $H \leq 100$ km which Occurred during the Period from 1964 to 1982 in the World
- Fig. 7-6 Epicenters of Earthquakes of Magnitude : $M \geq 4$ and Focal Depth : $H \geq 100$ km which Occurred during the Period from 1964 to 1982 in the World
- Fig. 7-7 Lithospheric Plates and Microplates in North-eastern to Middle Asia and the Direction of Micro Plate Movements relative to the India-Eurasia Collision
- Fig. 7-8 Epicenters of Earthquakes Occurred in Asia
- Fig. 7-9 Average Positions of Pressure Axes in Southeast Asia
- Fig. 7-10 Average Positions of Tension Axes in Southeast Asia
- Fig. 7-11 Distribution of Shallow Earthquakes ($M \geq 6$) since 1900
- Fig. 7-12 Asismic Area in Asia
- Fig. 7-13 Distribution of Epicenters of Strong Earthquake and Structural Lines in Asia
- Fig. 7-14 Epicentral Distribution of Earthquake within 500 km Radius from Mae Lama Luang Damsite
- Fig. 7-15 Epicenters of Earthquakes ($3.0 \leq M \leq 4.5$) within 1,000 km Radius from Mae Lama Luang Damsite

- Fig. 7-16 Epicenters of Earthquakes ($4.5 \leq M \leq 5.0$) within 1,000 km Radius from Mae Lama Luang Damsite
- Fig. 7-17 Epicenters of Earthquakes ($5.0 \leq M \leq 6.0$) within 1,000 km Radius from Mae Lama Luang Damsite
- Fig. 7-18 Epicenters of Earthquakes ($6.0 \leq M \leq 7.0$) within 1,000 km Radius from Mae Lama Luang Damsite
- Fig. 7-19 Epicenters of Earthquakes ($7.0 \leq M \leq 8.5$) within 1,000 km Radius from Mae Lama Luang Damsite
- Fig. 7-20 Seismotectonic Map of Thailand and the Adjoining Regions
- Fig. 7-21 Seismicity Map around Mae Lama Luang Damsite
- Fig. 7-22 Projections of the Locations of Earthquakes and Fault Plant Solutions
- Fig. 7-23 'Time Lag' between Impoundment and First RIS Event
- Fig. 7-24 'Time Lag' between Impoundment and Larger RIS Event
- Fig. 7-25 Magnitude of the Largest RIS Event Versus 'Time Lag' of accepted Cases of RIS
- Fig. 7-26 Magnitudewise Distribution of reported RIS Cases
- Fig. 7-27 Annual Distribution of the Earthquakes ($M \geq 3.0$) within 1,000 km in Radius from Mae Lama Luang Damsite (1964 - 1971)
- Fig. 7-28 Annual Distribution of the Earthquakes ($M \geq 3.0$) within 1,000 km in Radius from Mae Lama Luang Damsite (1972 - 1979)
- Fig. 7-29 Annual Distribution of the Earthquakes ($M \geq 3.0$) within 1,000 km in Radius from Mae Lama Luang Damsite (1980 - 1987)
- Fig. 7-30 Seismicity of All Data in 1901 - 1987
Total Number of Plots in the Area of $D \leq 1,000$ km is 1,107
- Fig. 7-31 Return Period for Maximum Acceleration Estimated
by Eq.-(1) [Oliveira]

- Fig. 7-32 Return Period for Maximum Acceleration Estimated
by Eq.-(2) [McGuire]
- Fig. 7-33 Return Period for Maximum Acceleration Estimated
by Eq.-(3) [Esteve & Rosenblueth]
- Fig. 7-34 Return Period for Maximum Acceleration Estimated
by Eq.-(4) [Katayama]
- Fig. 7-35 Comparisons of Various Attenuation Models ($M = 7.0$)
- Fig. 7-36 Regional Distributions of the Maximum Earthquake Motion in and
around Thailand. V_{max} for Return Period $T_r = 50$ Years.
- Fig. 7-37 Seismic Risk Map in and around Thailand
 V_{max} for Return Period $T_r = 100$ Years.
- Fig. 7-38 Seismic Risk Map in and around Thailand
 V_{max} for Return Period $T_r = 200$ Years.
- Fig. 7-39 Seismic Risk Map in and around Thailand
 A_{max} for Return Period $T_r = 50$ Years.
- Fig. 7-40 Seismic Risk Map in and around Thailand
 A_{max} for Return Period $T_r = 100$ Years.
- Fig. 7-41 Seismic Risk Map in and around Thailand
 A_{max} for Return Period $T_r = 200$ Years.
- Fig. 7-42 Seismic Zoning Map for Thailand and the Adjacent Regions

CHAPTER 7 SEISMICITY

7.1 General

The Mae Lama Luang dam is located about 5 km east of the Moei river which defines the border between Thailand and Myanmar, at the east side of Himalayan orogenic zone. Numerous tectonic lines (NNW-SSE) are widespread in this area and the most conspicuous faults among them are the Tounggy fault (in Myanmar) and the Moei-Uthai Thani fault (in Thailand).

The Moei-Uthai Thani fault was investigated in detail by EGAT and a report was submitted as "Tentative Report on Seismicity Study of Nam Yuam Project", Geology Section, Survey and Ecology Department, EGAT, February 1989.

JICA also performed the field survey with the geologists of EGAT to investigate the Moei-Uthai Thani fault.

Outline of tectonics and seismicity of the Project Area with the result of the field survey are described below and the list of references used in this study is attached in Appendix.

7.2 Structural Geology

7.2.1 Geological Outline

The project area which includes Mae Lama Luang and Nam Ngao damsites is located in lat. about $17^{\circ} 47'$ and long. $97^{\circ} 48'$ in the Mae Hong Son province in the northwest part of Thailand. The report, "Evaluation of Seismicity in the Kanchanaburi Province", prepared for EGAT by EBASCO in June 1984, explains the tectonic situation of Thailand as follows:

"On the basis of geology, morphology, and tectonic history, Thailand can be subdivided into three major parts: 1) Eastern Thailand, represented by the Korat Plateau, 2) the depression of the Gulf of Thailand and its extension northward as the central valley, and 3) the western and northern mountain belt that continues southward into the mountains of Malaysia."

According to the above mentioned report it is known that the project area belongs to the "Western and Northern Mountain Belt" described in 3). Further the report states, regarding the tectonic setting of the Western and Northern Mountain Belt zone, as follows:

"The western part of Thailand is currently in the transition zone between the active Himalayan continental collision belt to the northwest and ongoing oceanic subduction along the Indonesian arc to the south (Le Dain and others, 1984).

Within the Andaman Basin itself, analysis of instrumentally recorded seismicity suggests continued north-south extension along east-west spreading axes (Hutchinson, 1978). The spreading in the Andaman sea and the continuing movement and counterclockwise rotation of India (Eguchi and others, 1979; Chandra, 1981) is accommodated by right-lateral movement along major north-south trending strike-slip faults in Myanmar and the transform faults of the Andaman sea and the western coast of Sumatra (Asnachinda, 1978; Hamilton, 1979; Verma and others, 1979)."

The geology and the tectonics of the project area can be summarized as follows:

Various kinds of rocks belonging to the era from Lower Paleozoic to Mesozoic are observed in this area and the strikes of these formations show a conspicuous NW-SE direction.

The so-called Moei-Uthai Thani fault in Thailand which seemed to continue into Pan Laung- and Tounggy faults in Myanmar shows the direction of NW-SE which coincide with the direction of the formations.

The Moei-Uthai Thani fault zone is characterized by a narrow and complex fault zone of a normal, thrust and strike-slip natures. The horizontal displacement shows a left-lateral appearance.

7.2.2 Structural Geology of Thailand

The oldest rock in Indochina Peninsula region is the metamorphic base rock which was produced by the orogenic movement in Late Precambrian or Early Paleozoic. The orogenic movement in this region took place three times, as described below, in the period from Late Palaeozoic to the present.

<u>Orogenic Movement</u>	<u>Period</u>
1st : Hercynian	(Carboniferous)
2nd : Indochina	(Permian - Jurassic, mainly Triassic)
3rd : Himalayan	(Cretaceous - Quaternary)

The new orogenic belt was formed in the cocentric circle shape surrounding the old orogenic belt. The land called "Annamia" is considered to be formed in the Hercynian orogenic movement.

After that, the continent called "Indosinia" was formed around "Annamia" in Indochina period.

Most part of the original Indosinia continent still remain as a stable region at present.

General geological structure is shown in Fig. 7-1. And the schematic structural map of Thailand and the surrounding regions is shown in Fig. 7-2.

During the Silurian period, subduction of the ocean floor commenced along the eastern margin of the Shan-Thai Craton. Subduction to the west continued until the early Mesozoic, with the production of a series of superimposed volcanic arcs, as represented by andesitic and rhyolitic volcanics in central Thailand, extruded during Siluro-Devonian, Carboniferous-Early Permian, Late Permian-Early Jurassic and Late Triassic-Jurassic era. Collision of the Shan-Thai Craton with the Indosinian Craton took place during Triassic to Early Jurassic; but according to Burton (1984), the two cratons were in contact by Middle to Late Permian. The collision zone is represented by the Nan Suture in central Thailand.

The collision has produced the main geologic features of Thailand as linear deformation belts trending approximately north-south. Most

of the deformation belts (foldings and overthrustings) are controlled by fractures and/or curved faults. Major fault zones in the country are aligned in the NE and NW directions.

The bulk of the ranges are formed of thick turbiditic Cretaceous to upper Eocene shales and sandstones [Brunnschweiler, 1966; Mitchell, 1981]. The flysch is tightly folded all along the ranges but more intensely in the Naga Hills than farther south. It is generally accepted that the Indoburman ranges were formed in Cenozoic era as a result of subduction of the Indian plate under the Asian plate [Curry and Moore, 1974; Curry et. al., 1978; Mitchell, 1981]. During subduction, the thick turbidite prism with ophiolitic melanges was progressively thrust onto the Indian plate. Shortening apparently has taken place more or less continuously from the Late Cretaceous to the present. The flysch is overlain by Miocene deltaic or freshwater molasse along the western edge of the ranges [Curry and Moore 1974] (Fig. 7-2). In some areas on the eastern side of Arakan Yoma, metamorphic schists and ultrabasics (peridotites and diorites, serpentized to varying degrees and including chromite and nickel ore) have been overthrust westward onto the flysch (Fig. 7-2) [Brunnschweiler, 1966; Mitchell, 1981].

East of the "Shan scarp," the Shan Plateau rises above the central lowlands: its average elevation increases from 2,000 m in the south to 3,400 m in the northeast. Structurally, the Shan Plateau (and all the eastern highlands of Myanmar) belong to the Indochina platform, which probably collided with the South China platform in the Upper Triassic along what is now the Red River suture [Bunopas and Vella, 1978; Hamilton, 1979; Mitchell, 1981]. The basement of the plateau is composed of Precambrian granites, gneisses and schists [Maung Thein, 1973; Mitchell, 1981]. It is likely that two main blocks compose Indochina (the Shan, northwest Malaysia block, and the Khorat, southeast Malaysia block) and that they sutured in Early Mesozoic [Bunopas and Vella, 1978; Hamilton, 1977; Mitchell, 1977, 1981; Sengor, 1981; Stocklin, 1980]. This inference is supported by the existence of a zone with ophiolites and melanges, which divides both Indochina and the tip of the Malay Peninsula (Fig. 7-2) and is bordered mostly to the west by Late Paleozoic and Early Mesozoic

(Permo-Triassic) granites and acid volcanics. Upper Mesozoic deposits over most of the Indochina block are continental or shallow marine. Folding and metamorphism occurred in Jurassic in the western part of the Shan Plateau [Mitchell, 1981], but the tabular red beds of the Khorat Plateau to the east (Fig. 7.2) are essentially undeformed. In the Shan Plateau and Malay Peninsula the most recent intrusives are found in the west [Beckinsale et. al., 1979; Bignell and Snelling, 1977]. Thus magmatic and tectonic activity seem to have migrated to the west during Mesozoic [Hamilton, 1979; Mitchell, 1981].

7.2.3 Major Faults in Thailand

Figure 7-3 shows the major faults in western Thailand. Although in the surrounding region a few minor faults exist, right at the epicentral area no active fault could be confirmed (EGAT, 1985). Therefore, any release of large seismic energy at this locality appears to have little direct relation to a fault movement. However, the area is probably in a highly stressed condition because of the movements of the two major faults -- the Three Pagoda fault and the Moei-Uthai Thani fault, particularly the former one -- passing at a little distance from the present epicenter (Fig. 7-3). The drainage system around the present epicentral vicinity also follows the trend of the Three Pagoda fault. The Moei-Uthai Thani and Three Pagoda faults are prominent structures in the area. They trend several hundred kilometers along the NW-SE direction. Both of them are considered to have some relation with the Shan Scarp fault in Myanmar at the NW end and the Klong Marui fault at SE (not in the figure).

Although these two right-lateral faults used to be designated as inactive faults of the past, their influence on local geological structures is quite conspicuous. This is further corroborated by the analysis of the surface joint pattern. However, there are some evidences that these two major faults are in a process of reactivation since Late Tertiary. The Moei-Uthai Thani and Three Pagoda faults are believed to be originated during the earlier mentioned Triassic-Jurassic collision of the Shan-Thai Craton with the Indosinian Craton. Jurassic-Cretaceous tectonism of western Thailand is dominated by the activities of these two faults. Then afterwards, they probably became gradually inactive. Again during Late Tertiary, which coincides with the collision of the Indian plate with the Eurasia, they probably began to be active. In fact, the India-Eurasia collision changed the tectonic regime of Thailand; it might have halted the clockwise motion of south China. In the absence of the twisting stress, southeast Asia probably relaxed, resulting in the deposition of the Tertiary basin forming the Gulf of Thailand and causing its subsequent northward extension (Bunopas and Vella, 1983).

7.2.4 Moei-Uthai Thani Fault

As previously stated, the strike of the so-called Moei-Uthai Thani fault shows a distinct NW-SE direction which well coincides with the geological structure in this area. This fault may not be a continuous single line fault, but a complex fault which consists of a number of faults with similar NW-SE directions.

At two locations we observed large scale outcrops during our field work which looked like cataclasite. The reticulate micro cracks observed on the outcrops may be due to extreme stress. Since the locations of those outcrops are consistent with the position of the Moei-Uthai Thani fault on the geological map, the extreme stress that acted on the rock mass could be judged to have been caused by fault movement. Therefore, it is a high possibility to interpret that these outcrops are situated on some part of the Moei-Uthai Thani fault zone.

Admitting that it is so, the activity of this fault remains unsolved. To investigate the activity of this fault, a detailed geological survey around the fault, especially the detailed examination of the state of distribution of the Quaternary deposits must be done in the next stage.

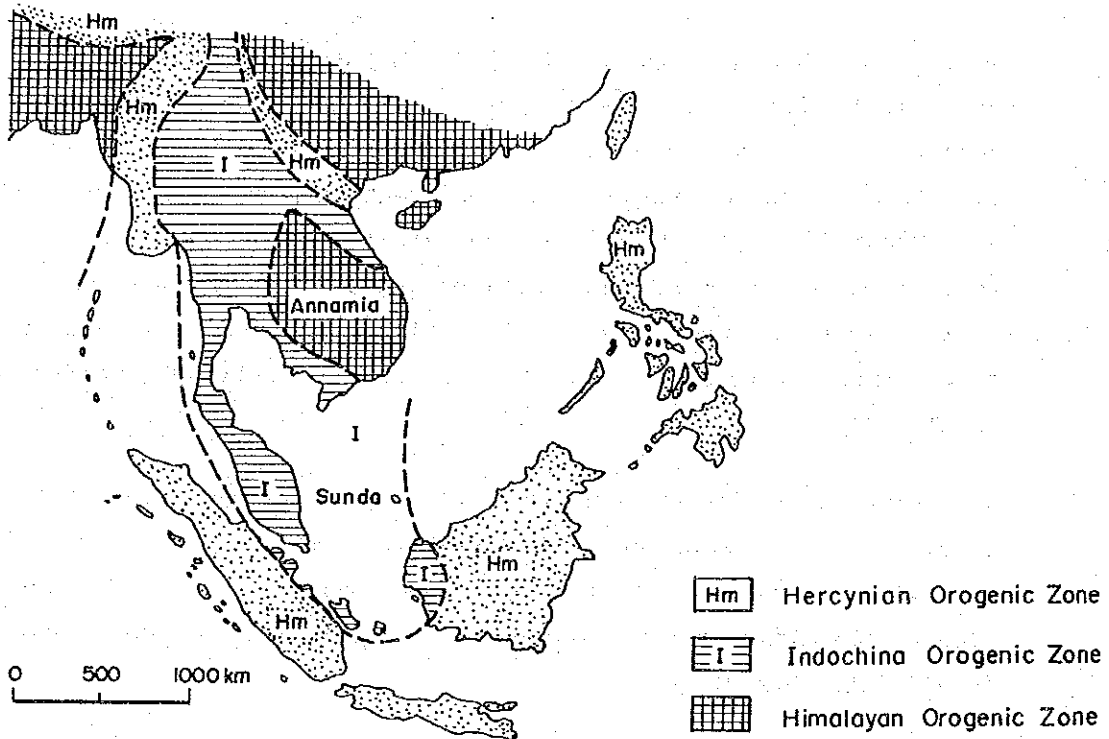


Fig. 7-1 General Geological Structure of Southeast Asia

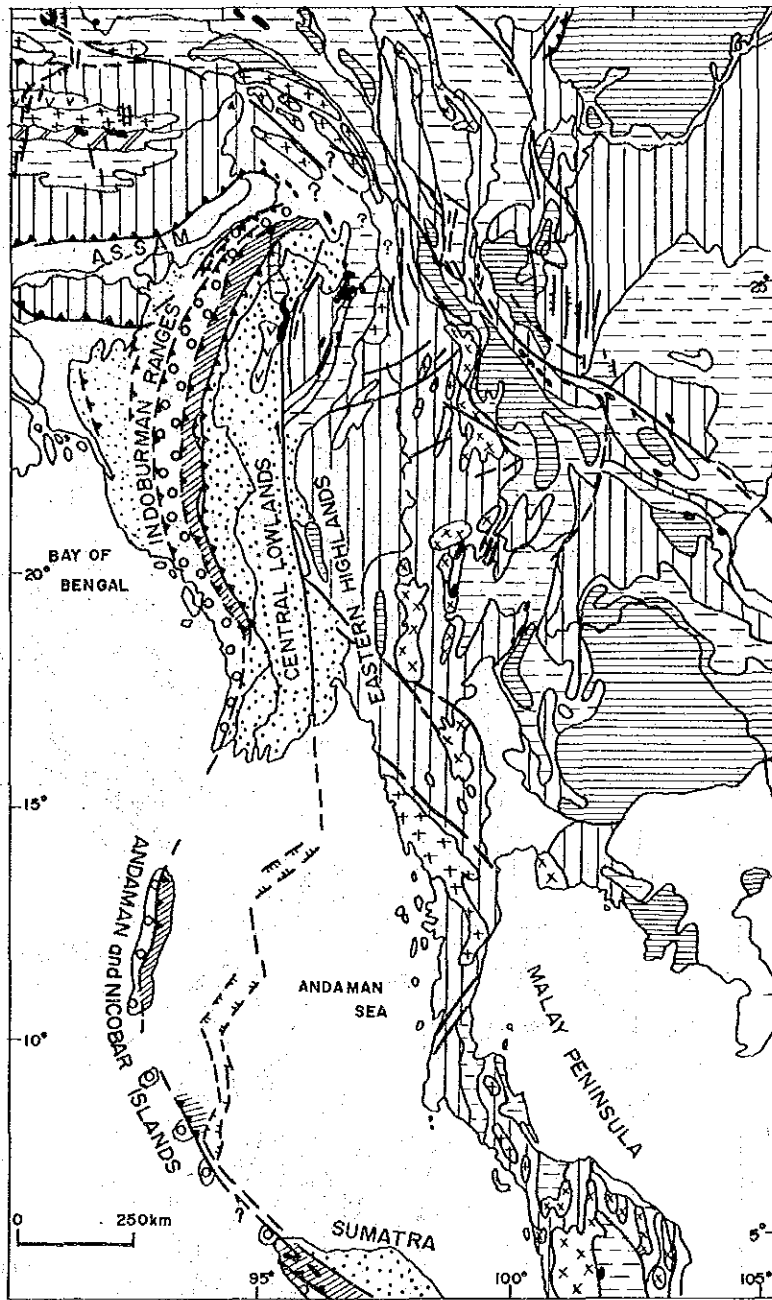


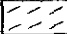
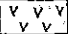

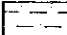
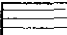
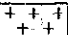
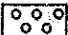

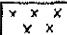







Fig. 7-2 Schematic Structural Map of Thailand and Surrounding Regions
(after Le Dain et al (1984))

(Legend)

 Oligocene Molasses	 Indus-Triassic flysch	 Metamorphic complex (Naga Hills in particular)	 Tertiary volcanics
 Eocene to Pleistocene molasses of the Burma Lowlands	 Mesozoic, including Lower Mesozoic flysch	 Upper Mesozoic platform sediments	 Middle to late Mesozoic granites
 Eocene flysch (with exotic blocks at places)	 Paleozoic and Proterozoic	 Late Paleozoic to Early Mesozoic granites	 Strike slip
 Flysch and melanges with exotic blocks	 Onhiolites		 Major Fault overthrusts
			 Normal

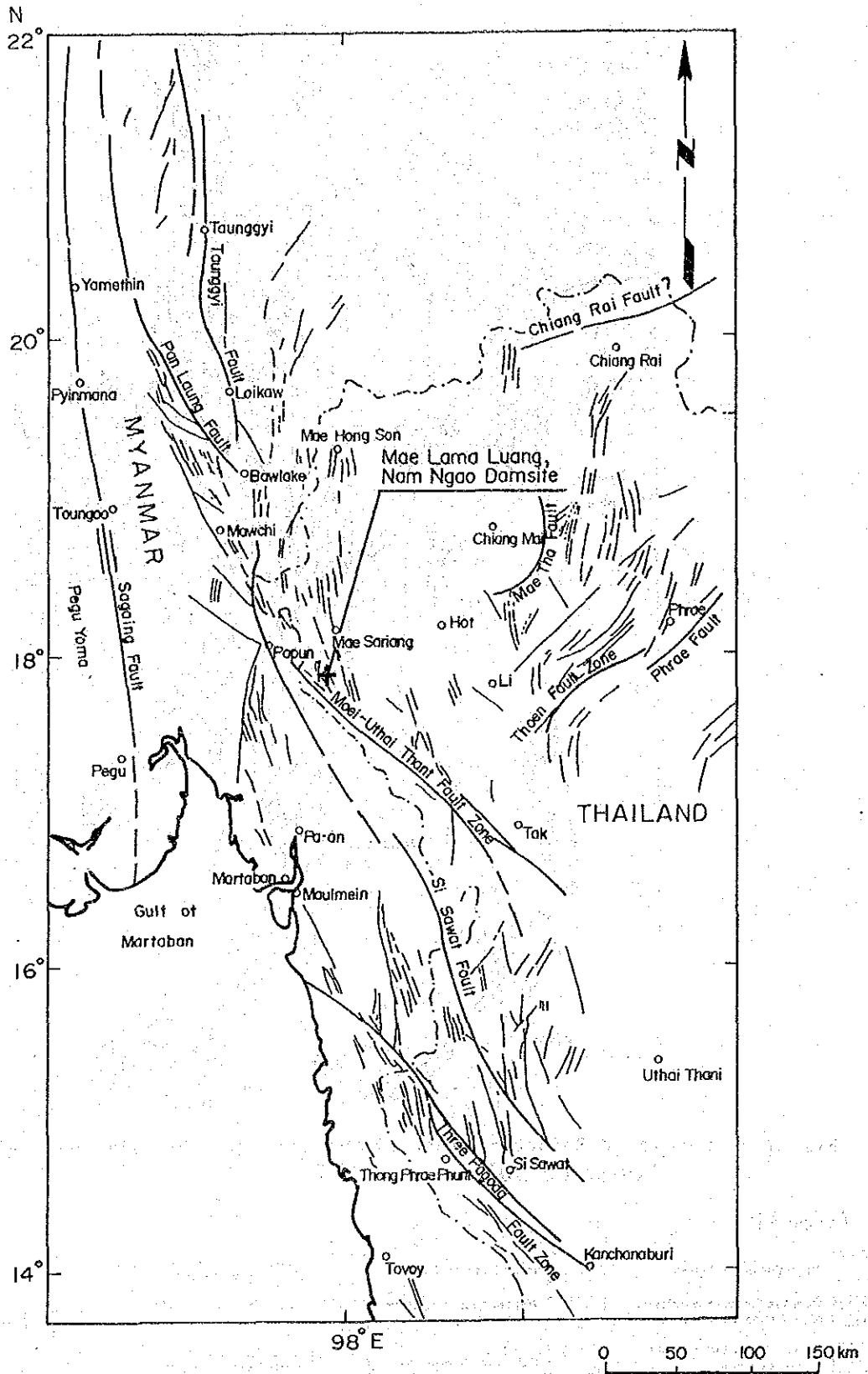


Fig. 7-3 Major Faults in the North-Western Part of Thailand

("Southeast Asia Association of Seismology and Earthquake Engineering"
Series on Seismology Volume II, Thailand 1985)

7.3 Seismicity of Thailand

7.3.1 Tectonic Plates and Seismicity

The earthquake phenomena has not only the physical side as a destruction phenomena of rock but also the physical geographical side as a result of tectonic movement. The individual great earthquakes are the exact results of the tectonic movement, and the moderate-small earthquakes concentrated at a certain limited area reflect the characteristics of the mobil belt. Accordingly, in order to clarify the earthquake phenomena, it is necessary to study about the characteristics of the rock destruction, the mechanism of the earthquake fault movement, the statistical characteristics of the earthquake occurrence, and finally to make clear the relationship between the tectonic movement and seismic activity.

The distribution of major tectonic plates on the earth and the plate boundaries is shown in Fig. 7-4. And the epicenters of the earthquakes of magnitude 4 or over which occurred in the world during the period from 1964 to 1982 are shown in Fig. 7-5 for focal depth shallower than 100 km and Fig. 7-6 for focal depth deeper than 100 km.

It is clear that the earthquakes occur mainly at the plate boundaries as a result of tectonic movement, or interaction between tectonic plates as seen in Fig. 7-4, 7-5 and 7-6.

The lithospheric plates and microplates around Thailand and the direction of the microplate movements relative to the India - Eurasia collision are shown in Fig. 7-7. And the epicenters of earthquakes occurred in Asia is shown in Fig. 7-8. High seismic zone is distributed limitedly along the plate boundaries. While the stable and low seismic zone is widely distributed inside of the plates. Most of the continental shield and the ocean floor form the stable and low seismic zone.

The most typical features of the plate tectonics evolution in the considered area are generally represented by the results of interaction between three major plates: the Eurasian, Pacific and Indo-Australian. The Eurasian plate is believed to be still, while

the Indo-Australian plate moves northward with a clockwise component and the Pacific plate moves essentially westward. Under the influence of this interaction the boundary of these plates and most of tectonic faults in the area are of trench and strike-slip fault types. Furthermore, two spreading centres situated in the Indian Ocean and in the East Sea, and two parallel opposing subduction zones were active at the same time, migrating towards the East Sea (from Trias to the present time). These features are reflected in the mechanism of earthquakes in the area.

The strike-slip motion is the main form of fault movement for shallow earthquakes. This is also a main type of tectonic faults in the area. For intermediate earthquakes the oblique-slip motion is a dominant form of movement in the focus.

7.3.2 Regional Stress Field around Thailand

The pressure axes and the tension axes of the earthquakes in south east Asia are shown in Fig. 7-9 and Fig. 7-10, respectively.

In southeast Asia, almost all structures and fault systems are directed to the northwest-southeast.

The area is divided into four smaller regions in Fig. 7-9. The first one contains the north Vietnam Mesozoic folding zone with the great Red River fault. All earthquakes in this region were in the Earth's crust. The second region is the western Myanmar Cenozoic folding zone with the chain of great faults which have direction either meridional or north-west-southeast. In this region a number of earthquakes occurred with depth reaching the upper mantle. The third region is the Cenozoic folding zone in the Andaman sea with meridional faults, where earthquakes occur in narrow bands in the Earth's crust or below. The fourth region is the part of the Cenozoic folding zone of Sumatra (Indonesia), belonging to the Asiatic earthquake belt of the Cenozoic tectonic belt of the Pacific Ocean. Most of earthquakes in this area occur in the subduction zone with depth reaching the upper mantle.

7.3.3 Seismicity in and around Thailand

With the development and spread of the modern earthquake observation network, the earthquakes of magnitude 5 or over which occurred all over the world can be observed without omission. Seismicity in Asia since 1900 can be drawn as shown in Fig. 7-11 by selecting the earthquakes of magnitude larger than 6 from the earthquake data file of the National Oceanic and Atmospheric Administration Environmental Data Service, USA (hereinafter NOAA).

As mentioned before, there exist two kinds of region classified according to the seismic activity, namely high seismic region and low seismic region. Aseismic region in Asia is shown in Fig. 7-12. Generally speaking, the earthquakes are not frequent in Indochina region, and Thailand can be considered to be a stable aseismic region, except its northern part.

Furthermore, the epicenters of the earthquakes of magnitude larger than 6 since 1500 and the main geological structures in Asia is shown in Fig. 7-13. Judging from the wide standpoint of view, it can be clearly said that Thailand is an aseismic country. Seismic activity of Thailand is remarkably low compared with the adjacent countries, or Myanmar, India, China, Nepal, Japan and so forth.

7.3.4 Seismic Activity around the Project Site

The epicentral distribution of the earthquakes within 500 km radius from the Mae Lama Luang dam site is shown in Fig. 7-14. It can be understood from this figure that the greater part of the earthquakes felt around the project area occurred in Myanmar and the Andaman sea.

The epicenter of the earthquakes classified according to the magnitude are shown in Fig. 7-15 ($3.0 \leq M \leq 4.5$), Fig. 7-16 ($4.5 \leq M \leq 5.$), Fig. 7-17 ($5.0 \leq M \leq 6.0$), Fig. 7-18 ($6.0 \leq M \leq 7.0$), and Fig. 7-19 ($M \geq 7.0$).

In Thailand, the earthquake of magnitude greater than 6 did not occur during the period from 1900 to 1987.

The seismotectonic map of Thailand and the adjoining regions is shown in Fig. 7-20, and the major historical earthquakes occurred near Thailand is listed in Table 7-1.

Furthermore, seismicity map around the Mae Lama Luang dam site and the projections of the locations of the earthquake fault plane solutions are shown in Fig. 7-21 and Fig. 7-22, respectively. The earthquakes determined their fault plane solutions are listed in Table 7-2.

Several large historic earthquakes seem to have been associated with continued activity in this area. Extensive changes of level on the Myanmar coast apparently were caused by the great Arakan earthquake of April 2, 1762 [Richter, 1958]. Then, following an earthquake in 1878, uplift of 6 m ("20 ft") occurred on the west coast of Ramree island (19°20'N), while another island farther north, False Island, seems to have disappeared [Richter, 1958]; the maximum intensity, however, appears to have been farther east. In 1881, a large event west of the Andaman Islands generated a small tsunami (Table 7-1).

Shallow and intermediate depth earthquakes occur in the Naga Hills, Chin Hills, and Arakan Yoma [Gutenberg and Richter, 1954; Santo, 1969] (Fig. 7-20).

The distribution of intermediate depth events shows a single, inclined zone dipping east of about 45° beneath the Indoburman ranges and therefore suggests the existence of a subducted slab of oceanic lithosphere under the eastern part of the ranges as shown in Fig. 7-22.

Recent tectonics, seem to have affected essentially two regions: southwest of Chiang Mai and the northern Shan Plateau (Fig. 7-20). Fault plane solutions of shallow earthquakes in these two areas support the idea that conjugate strike-slip faulting characterizes the active tectonics.

In the south about 100 km north of Moulmein, a major fault system, called Moei-Uthai Thani fault, extends for about 400 km in a north-

west direction past the city of Papun and transects the Mesozoic granites and gneisses (Fig. 7-2, Fig. 7-20). Assuming that the earthquake of February 17, 1975 (event 12), took place on it, the corresponding fault plane solution indicates a component of right-lateral motion on a north-west trending plane. In Thailand the fault splays into several parallel fault segments that "disappear" into Tertiary sediments farther south. East of Moulmein a prominent escarpment, which coincides roughly with a limit between Carboniferous sediments and basement and intrusives has the morphology of a normal fault (Fig. 7-20). The orientation of such a normal fault is consistent with right-lateral slip on the Moei-Uthai Thani fault and the other faults to the south. The tectonic style of the region would thus be qualitatively similar to that in the Andaman basin, with a mixture of strike-slip and normal faulting. Although its direction is different (Fig. 7-20), the Moei-Uthai Thani fault may take up some of the right-lateral displacement near the southern end of the Sagaing fault.

Main features regarding the earthquake mechanism around Thailand and the seismicity of Thailand can be summarized as follows:

The seismic evidences presented in historic record indicate a clear existence of plate boundary along the mountain front of Myanmar through the western margin of Andaman sea and the eastern part of Sunda arc.

The seismic slip at shallow depth associated with active zone of thrust faulting along the front arc accounts for the Indian ocean plate underthrusting the Eurasian plate. The distribution of stress represented by the maximum compression axis horizontally oriented in the northeast well corresponds to the present plate tectonic in this region. The zonally vertical cross-section of seismic activity shows the intermediate-depth earthquakes are distributed in a narrow zone along the mountain range of Myanmar and the western part of Andaman sea. The vertically inclie seismicity dipping eastward to the depth about 180 km implies the Indian ocean plate subducting beneath the Eurasian plate along the northwestern Sunda arc.

Shallow earthquake activity in the Andaman basin shows a clear lineament along the Nicobar rift valley through the Andaman-Nicobar ridge and the central Andaman trough.

Along the western margin of Andaman sea, shallow focus seismicity is distributed in a narrow zone. The right-lateral shear slip near the Nicobar rift valley is suggestive to a continuation of transcurrent fault in the decoupling zone from the Samangko fault on the Sumatra island.

Thailand is located in the east to a distance from the seismically active arc zone. Thailand may consider to be in aseismic zone located in the east about 400 km from the active central Andaman trough. The seismic activity sparses in the northern and western part of Thailand. The geological structure in this region described by Peter [1969] and Moore [1980] that belong to the folding mountain system which extends from the Shan Plateau in Myanmar through the Malay Peninsula. The major orogenesis of these folded belts occurred during the Triassic and Jurassic period in the northern and western part of Thailand, the Triassic and Jurassic folding mountains are characteristic of disharmonic movement which due to the heterogeneity of rock and its overburden pressure. These result in an intense of folding and steep faulting which their strikes are more or less parallel to the structure axis trending in the north-south to northwest-southeast.

Earthquakes in the vicinity of Thailand from the contemporary record are located in the areas of intense thrust fault. The strong events have been around magnitude of 5 and ever caused some slight damage (September 1, 1978, 20.4°N 100.6°E, Felt I = iv in Chiang Rai Province, February 10, 1980, 19.4°N 99.2°E, Felt I = iii in Chiang Mai Province and December 22, 1980, 18.0°N 100.1°E, Felt I - iv in Phrae Province). Recently, the seismicity seem to increase in the western part of Thailand, there occurred 3 events with magnitude greater than 5 within duration of a week in April 1983. Since these earthquakes with moderate magnitude located near the dam site which consists of 2 major dams constructing over the Quae Yai and Quae Noi river. The Srinagarind dam has completed and started to impound water since 1977. In 1979, Makedr has mentioned the possibility of

earthquake activity increasing in this area related to the geological factor and the characteristic of the reservoir.

7.3.5 Seismic Events in 1983

(1) General Features of Reservoir Induced Seismicity

Koyna, Kariba, Kremasta, Hsinfengkiang, Aswan High, Oroville, Benmore, Encumbene, Hoover, Keban, Kurobe 4, Manicouagan 3, Nurek, Monteynard, Akosombo, Marathon, etc. are the dams which are famous for the reservoir induced seismicity. The representative reservoir induced earthquakes are listed in Table 7-3.

Regarding to the reservoir induced seismicity, some hypotheses have been proposed by many researchers. The main features of the reservoir induced seismicity can be summarized as follows:

- The seismic activity seems to result mainly from the filling of the reservoir.
- The seismicity considerably increases after reservoir impoundment. Many of the reservoir induced seismicities occur after 1 to 5 years from the start of impoundment. (Fig. 7-23 - Fig. 7-25)
- The seismic activity increases and diminishes with water level fluctuation. When the water level is low, the intensity of seismic activity and energy release reduces.
- The seismicity is not directly related to the stored volume of water, since a great number of large reservoirs does not show any seismicity.
- Sometimes, the seismicity seems to be related to the reservoir filling rate.
- The most frequented magnitude range is between 2.0 to 5.0 (Fig. 7-26).

- The maximum magnitude of the reservoir induced seismicity is considered to be 6.5 or 7.0.
- The reservoir induced seismicity tends to occur when the reservoir water depth is greater than 100 m.
- Epicentral distance of the reservoir induced seismicity is mostly less than 25 km.
- Focal depth of the reservoir induced seismicity is mostly shallower than 3 km, approximate ranging from 1 to 7 km.
- Most of the reservoir induced seismicity are situated in moderate to low seismic regions.
- The reservoir induced seismicity might be accompanied with normal or strike slip faulting.
- The maximum magnitude and intensity of shocks related to reservoir impoundment, generally do not exceed the natural seismicity levels.

The principal mechanism of the reservoir induced seismicity can be summarized as follows:

- The reservoir load generates stresses and provides the "last straw" for the seismogenic movements.
- The increase in pore pressure following impoundment reduces the effective stress necessary for crustal readjustments.

$$P = P_o - P_l$$

(Effective Stress) (Tectonic Stress) (Pore Pressure)

- The reservoir load itself causes the earth movement.

(2) Seismicity at Srinagarind Reservoir

Annual distributions of the earthquakes ($M > 3.0$) within 1,000 km in radius from the Mae Lama Luang dam site are shown in Fig. 7-27 to Fig. 7-29. In 1983, the earthquake swarm of medium to small magnitude occurred near the Srinagarind reservoir, as shown in Fig. 7-29.

Thailand, excepting its northern part, is located in the stable and aseismic region of the Indo-China peninsular. The release of significant seismic energy is a comparatively rare phenomenon here. However, the inland earthquake of M_p 5.8 occurred in the vicinity of the Srinagarind reservoir in April 22, 1983, accompanying 19 foreshocks and more than 300 aftershocks of magnitude greater than 2.0. The focal depths mostly concentrated between 8 km and 12 km. Regarding these events, the following results are reported by Ghose and Oike, 1987.

These particular earthquakes around the Srinagarind reservoir have no direct relation to the subduction or the back arc spreading processes operating in the western side of Thailand. They have occurred probably due to the release of accumulated internal strain through a local zone of weakness.

Primarily because of the action of the two major faults, the Three Pagoda fault and the Moei-Uthai Thani fault, the basement rock in the epicentral region was in a prestressed condition. In such circumstances, the water in the Srinagarind reservoir served as an additional factor to weaken the basement formation and thereby reduce the frictional resistance. The accumulated strain was finally released causing the seismicity. The basement rock corroded chemically by the reservoir water is thought to be unique phenomenon at the Srinagarind reservoir.

The water in the reservoir acted on the basement physico-chemically for six years since start of the impoundment, particularly acted on the susceptible granites.

Table 7-1 Major Historical Earthquakes in and Near Thailand

Date	Location	Magnitude or Brief Description
Mar. 23, 1839	Near Mandalay	"Very destructive"
Feb. 6, 1843	Near 19 1/2°N, 95 1/2°E	Caused eruptions of mud volcanoes on Ramree Island
Oct. 30, 1843	Also near 19°N, 95°E	More violent than preceding event
Jan. 3, 1848	Also near 19 1/2°N, 95 1/2°E	Strongest shaking at location given, but following earthquake False Island (at 18°38'N 95°55 1/2'E) apparently disappeared, "no trace of it being seen after the 24th August"
Dec. 31, 1881	West of Andaman Islands	Caused small tsunami, 1 m peak to trough in height, felt in Myanmar, Bengal, and India and damaging on Andaman, Nicobar Islands
May 23, 1912	21°N, 97°E	M = 8, I _{max} = IX; numerous foreshocks and aftershocks; zone of intensity VII elongated in a north-south direction parallel to Kyaukkuan fault; railroad tracks bent near fault but little deformed elsewhere
Jun. 22, 1923	22 3/4°N, 98 3/4°E	M = 7.3
Sep. 9, 1923	25 1/4°N, 91°E	M = 7.1
Mar. 16, 1925	25°N, 100°E	M = 7.1
Aug. 8, 1929	Near 19°N, 96 1/2°E	Bent railroad tracks, bridges and culverts collapsed, and loaded trucks overturned
May 5, 1930	17°N, 96 1/2°E	M = 7.3, I _{max} = IX, in a zone trending north-south for 70 km south of Pegu (therefore, parallel to the Sagaing fault)
Dec. 3, 1930	18°N, 96 1/2°E	M = 7.3, railroad tracks twisted
Jan. 27, 1931	25.6°N, 96.8°E	M = 7.6, I _{max} = IX; numerous fissures and cracks
Dec. 26, 1941	21°N, 99°E	M = 7.0
Oct. 23, 1943	26°N, 93°E	M = 7.2
Sep. 12, 1946	23 1/2°N, 96°E	M = 7 1/2
Sep. 12, 1946	23 1/2°N, 96°E	M = 7 3/4
Feb. 2, 1950	22°N, 100°E	M = 7.0

Descriptions, intensities, and qualified locations from Chhibber [1934]. Coordinates without prefix "near" and magnitudes from Gutenberg and Richter [1954].

Table 7-2 List of Selected Earthquakes
for Fault Plane Solutions

Event	Date	Location		H
		Lat(°N)	Long (°E)	
<u>Myanmar, South China, Laos, and Thailand</u>				
1.	Jan. 22, 1964	22.33	93.58	60
2.	Feb. 27, 1964	21.65	94.40	91
3.	Oct. 17, 1969	23.09	94.70	124
4.	Feb. 6, 1970	23.10	100.78	-
5.	Jul. 29, 1970	26.02	95.37	68
6.	Apr. 28, 1971	22.93	101.03	-
7.	May 30, 1971	25.23	96.44	-
8.	May 31, 1971	25.19	96.51	-
9.	Sep. 14, 1971	22.97	100.71	-
10.	Dec. 29, 1971	25.12	94.67	-
11.	May 31, 1973	24.28	93.55	-
12.	Feb. 17, 1975	17.64	97.90	-
13.	May 21, 1975	23.87	94.11	72
14.	Jul. 8, 1975	21.49	94.70	157
15.	May 29, 1976	24.57	98.95	-
16.	Jul. 21, 1976	24.78	98.69	-
17.	May 12, 1977	21.74	92.99	-
<u>Andaman Sea **</u>				
18.	Jul. 28, 1964	14.17	96.12	-
19.	Sep. 15, 1964	08.90	93.03	89
20.	Feb. 14, 1967	13.75	96.47	-
21.	Sep. 6, 1967	14.65	93.55	-
22.	Mar. 28, 1971	11.77	95.05	-
23.	Jul. 27, 1971	13.71	95.87	-
24.	Nov. 13, 1972	12.44	95.23	-
25.	Jul. 9, 1973	10.69	92.58	44
26.	Feb. 16, 1974a	11.43	92.35	-
27.	Feb. 16, 1974b	11.45	92.36	-
28.	Dec. 11, 1976	07.49	93.81	-

H, depth (km)

* Fitch [1970].

** Eguchi et al [1979]

Table 7-3 Representative Reservoir Induced Earthquakes

M	Dam	Nation	Dam Height (m)	Pondage (10 ⁸ t)	M of 1st RIS
M > 5	Aswan High	Egypt	111	1,600.0	5.6
	Kariba	Zambia, Rhodesia	128	1,603.7	5.8
	Koyna	India	103	27.8	6.5
	Kremasta	Greece	147	47.5	6.3
	Oroville	USA	236	43.0	5.9
	Hsinfengkiang	China	105	115.0	6.1
M ≤ 5	Benmore	New Zealand	118	20.4	5.0
	Encumbene	Australia	116	41.7	5.0
	Hoover	USA	221	367.0	5.0
	Keban	Turkey	207	30.6	3.5
	Kurobe 4	Japan	180	2.0	4.1
	Manicouagan 3	Canada	108	104.0	4.1
	Nurek	USSR	317	104.0	4.6

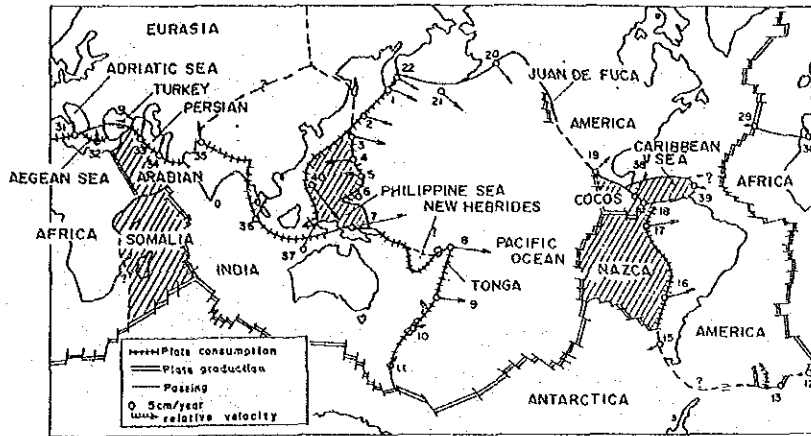


Fig. 7-4 Distribution of Major Tectonic Plates on the Earth and Plate Boundaries

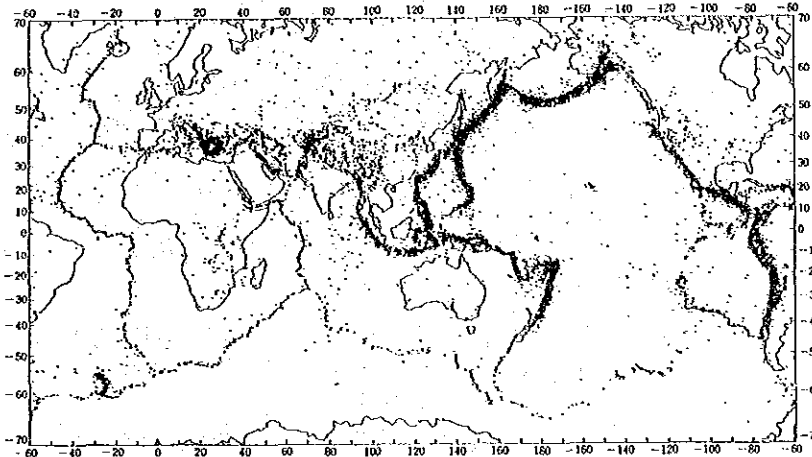


Fig. 7-5 Epicenters of Earthquakes of Magnitude : $M \geq 4$ and Focal Depth : $H \leq 100$ km which Occurred during the Period from 1964 to 1982 in the World

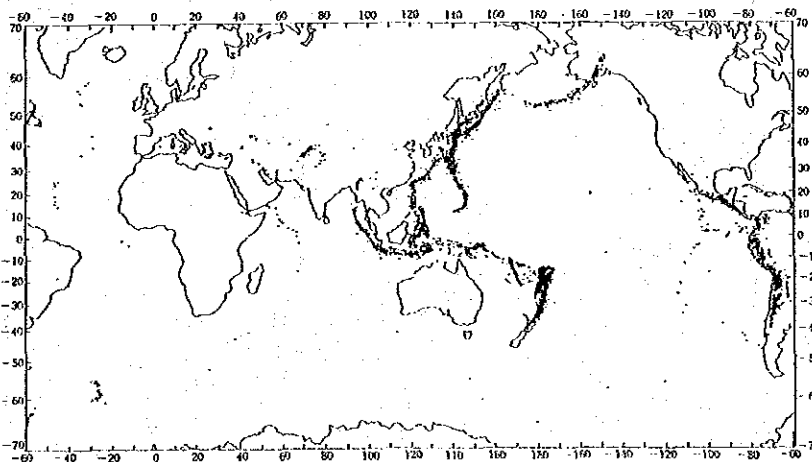


Fig. 7-6 Epicenters of Earthquakes of Magnitude: $M \geq 4$ and Focal Depth : $H \geq 100$ km which Occurred during the Period from 1964 to 1982 in the World

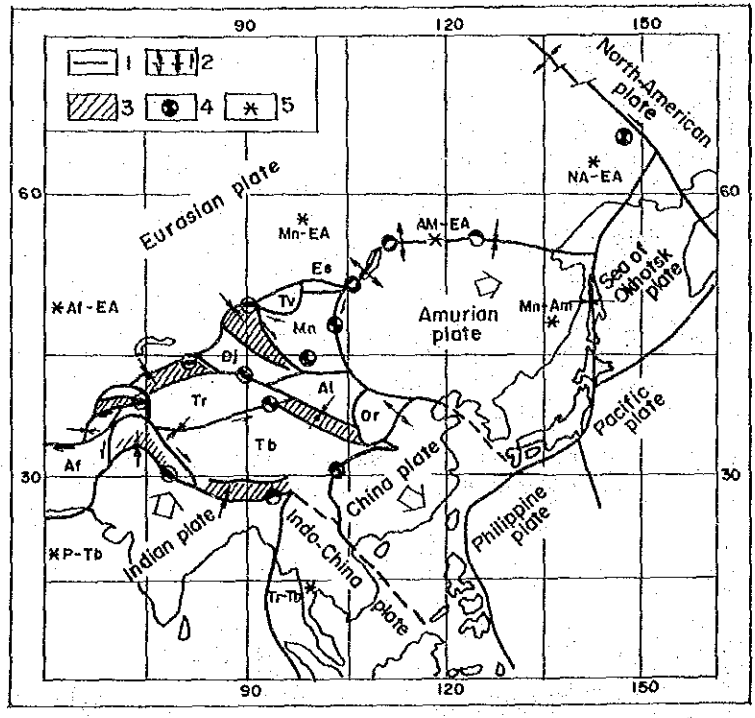


Fig. 7-7 Lithospheric Plates and Microplates in North-eastern to Middle Asia [after Zonenshain and Savostin (1981)] and the Direction of Micro Plate Movements relative to the India-Eurasia Collision

Al = Alashan , Af = Afghan , Dj = Dzungarian,
 Mn = Mongolian, Or = Ordos, P = Pamir,
 Tr = Tamir, Tb = Tibetan.
 Smaller blocks : ES = Eastan Sayan, Tu = Tuva,
 Td = Tadzhik , F = Fergana

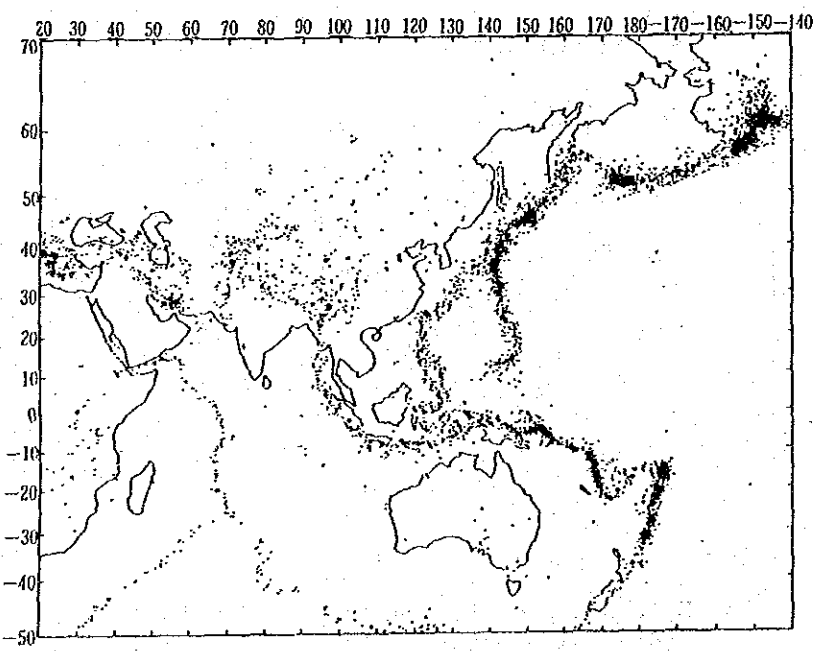


Fig. 7-8 Epicenters of Earthquakes Occurred in Asia

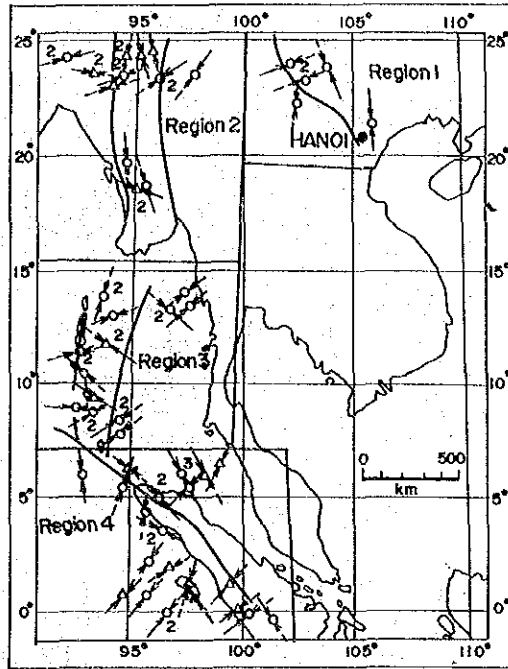


Fig. 7-9 Average Positions of Pressure Axes in Southeast Asia
 Black dots and triangles show the location of single epicenters for shallow and intermediate earthquakes, respectively. The earthquakes with almost identical mechanism are shown by the numbers next to their average positions. The longest arrows indicate the plunge from 0 to 30°, the medium arrows from 31 to 60°, and the shortest from 61 to 90°. The solid lines show the main geological faults. The project site is shown by the cross.

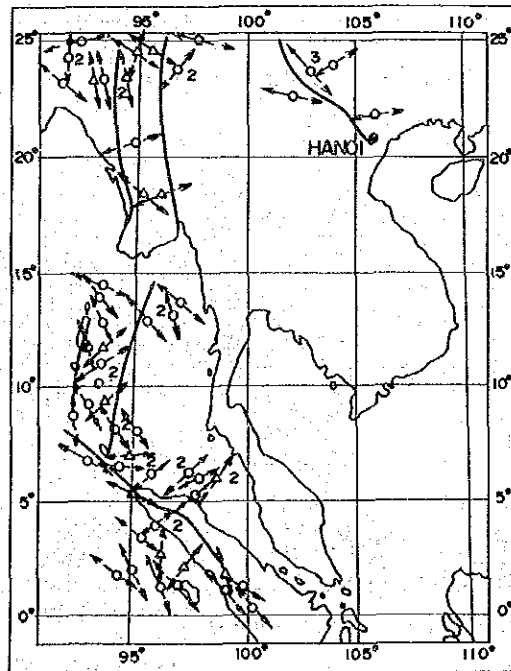


Fig. 7-10 Average Positions of Tension Axes in Southeast Asia
 The symbols are the same as in Fig. 7-9.

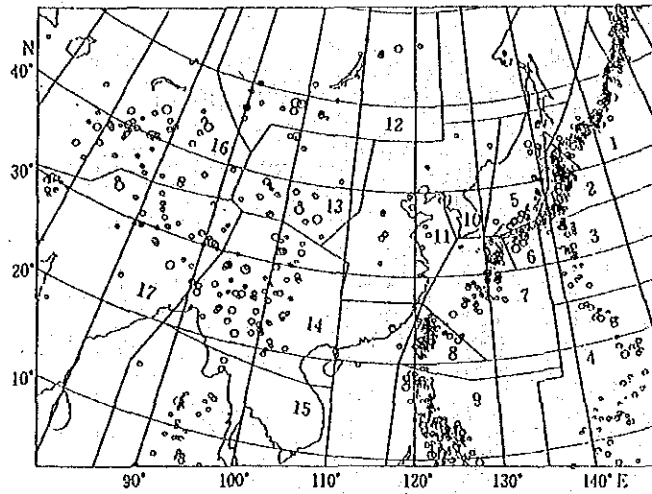


Fig. 7-11 Distribution of Shallow Earthquakes ($M \geq 6$) since 1900

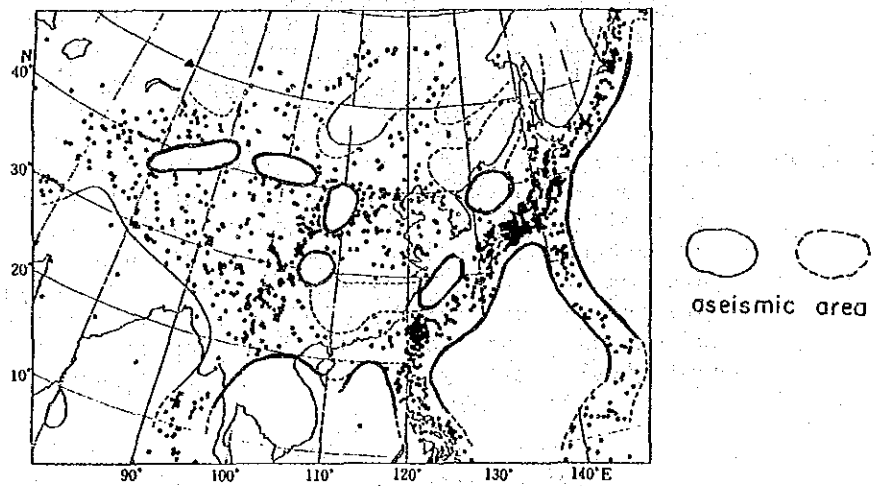


Fig. 7-12 Aseismic Area in Asia

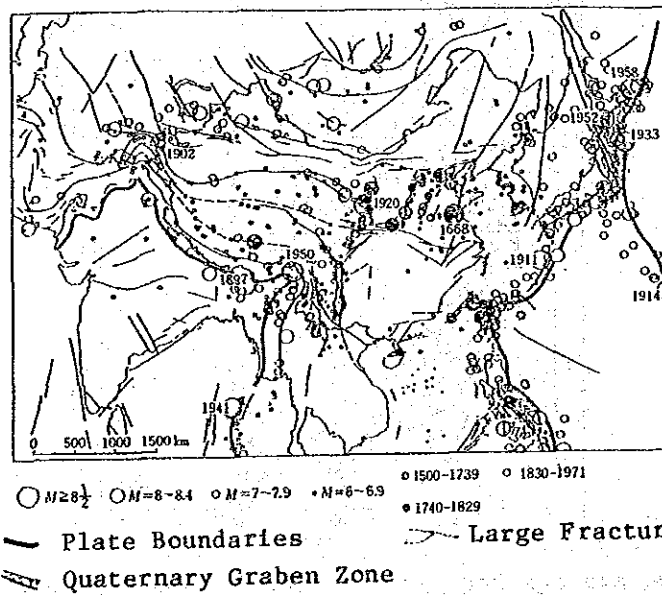


Fig. 7-13 Distribution of Epicenters of Strong Earthquake and Structural Lines in Asia

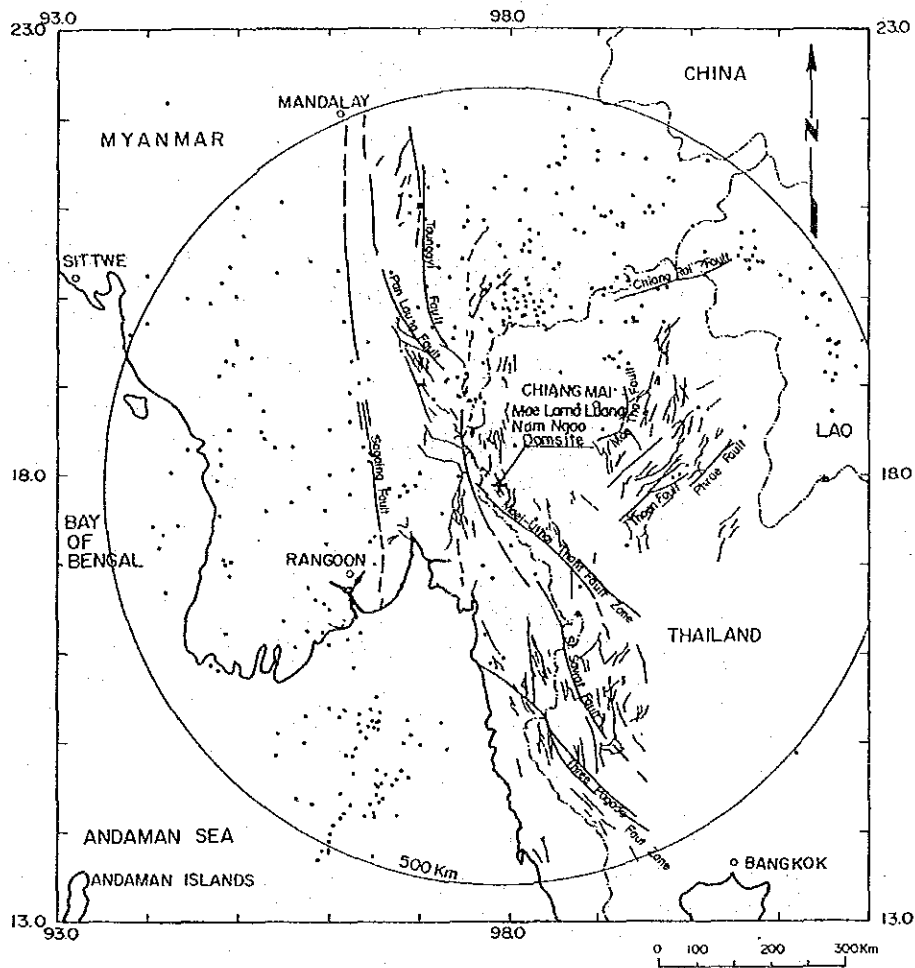


Fig. 7-14 Epicentral Distribution of Earthquake within 500 km Radius from Mae Lama Luang Damsite

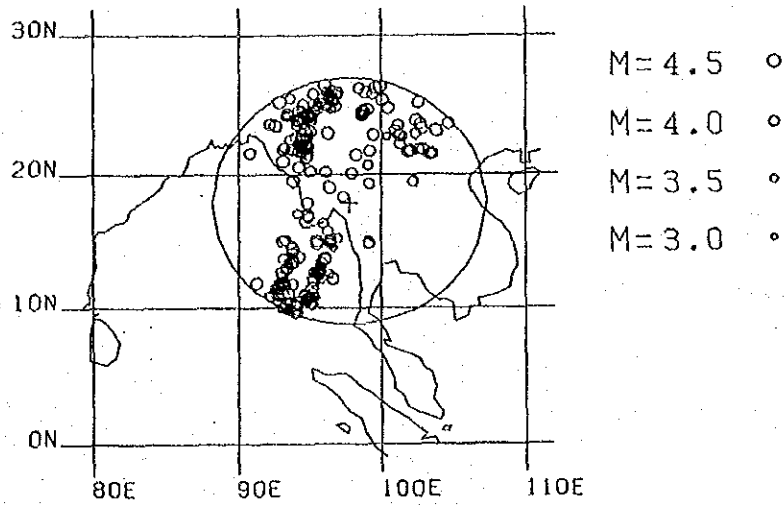


Fig. 7-15 Epicenters of Earthquakes ($3.0 \leq M \leq 4.5$) within 1,000 km Radius from Mae Lama Luang Damsite

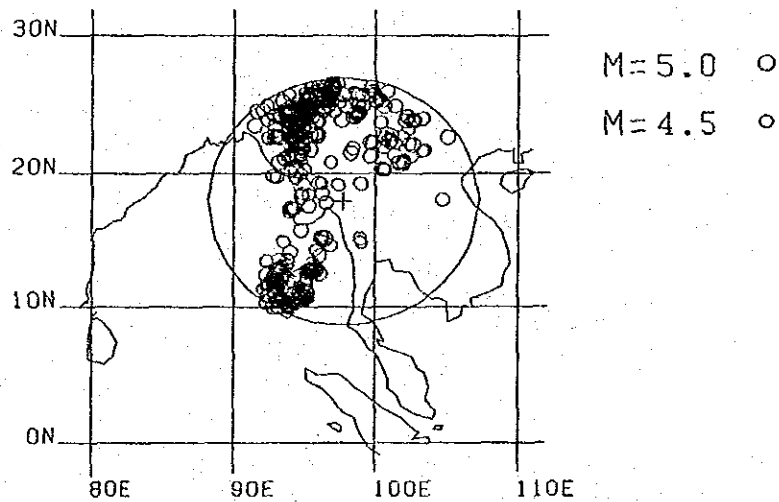


Fig. 7-16 Epicenters of Earthquakes ($4.5 \leq M \leq 5.0$) within 1,000 km Radius from Mae Lama Luang Damsite

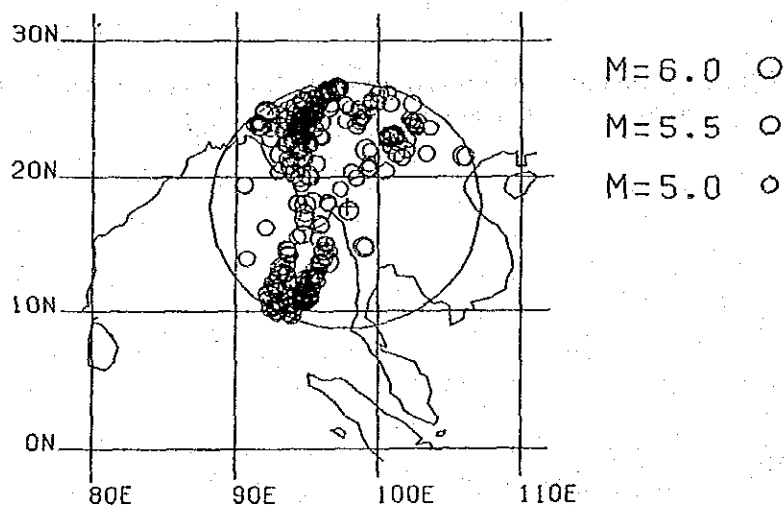


Fig. 7-17 Epicenters of Earthquakes ($5.0 \leq M \leq 6.0$) within 1,000 km Radius from Mae lama Luang Damsite

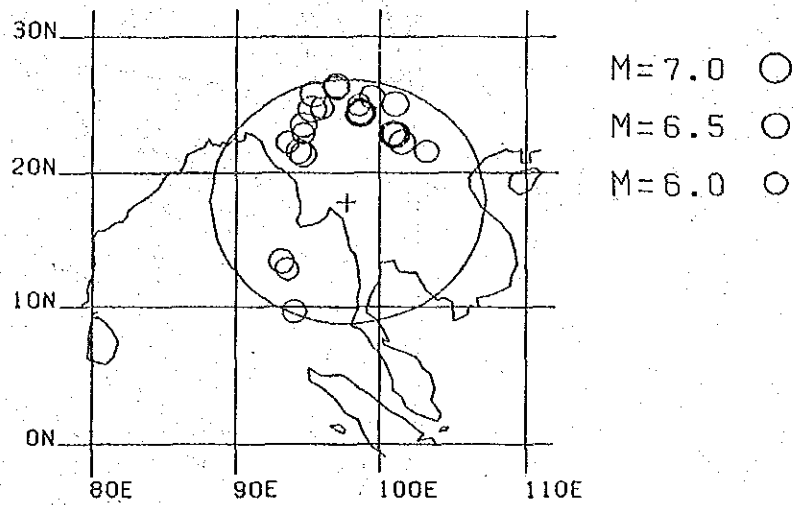


Fig. 7-18 Epicenters of Earthquakes ($6.0 \leq M \leq 7.0$) within 1,000 km Radius from Mae Lama luang Damsite

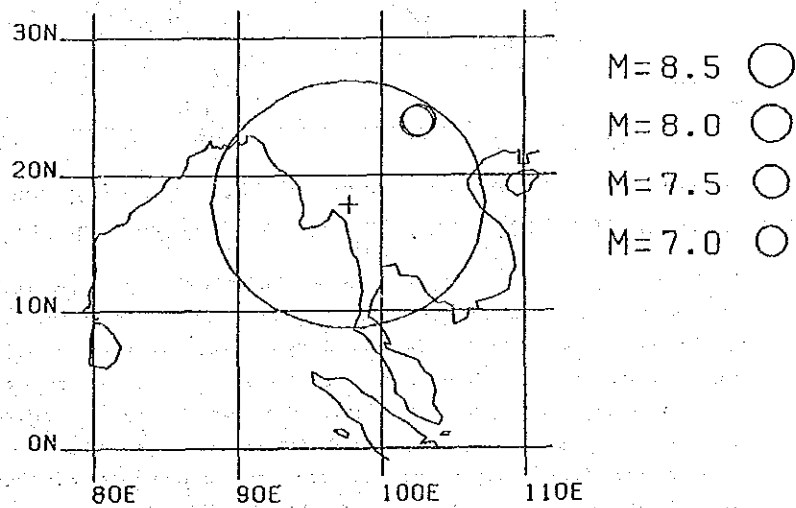


Fig. 7-19 Epicenters of Earthquakes ($7.0 \leq M \leq 8.5$) within 1,000 km Radius from Mae Lama Luang Damsite

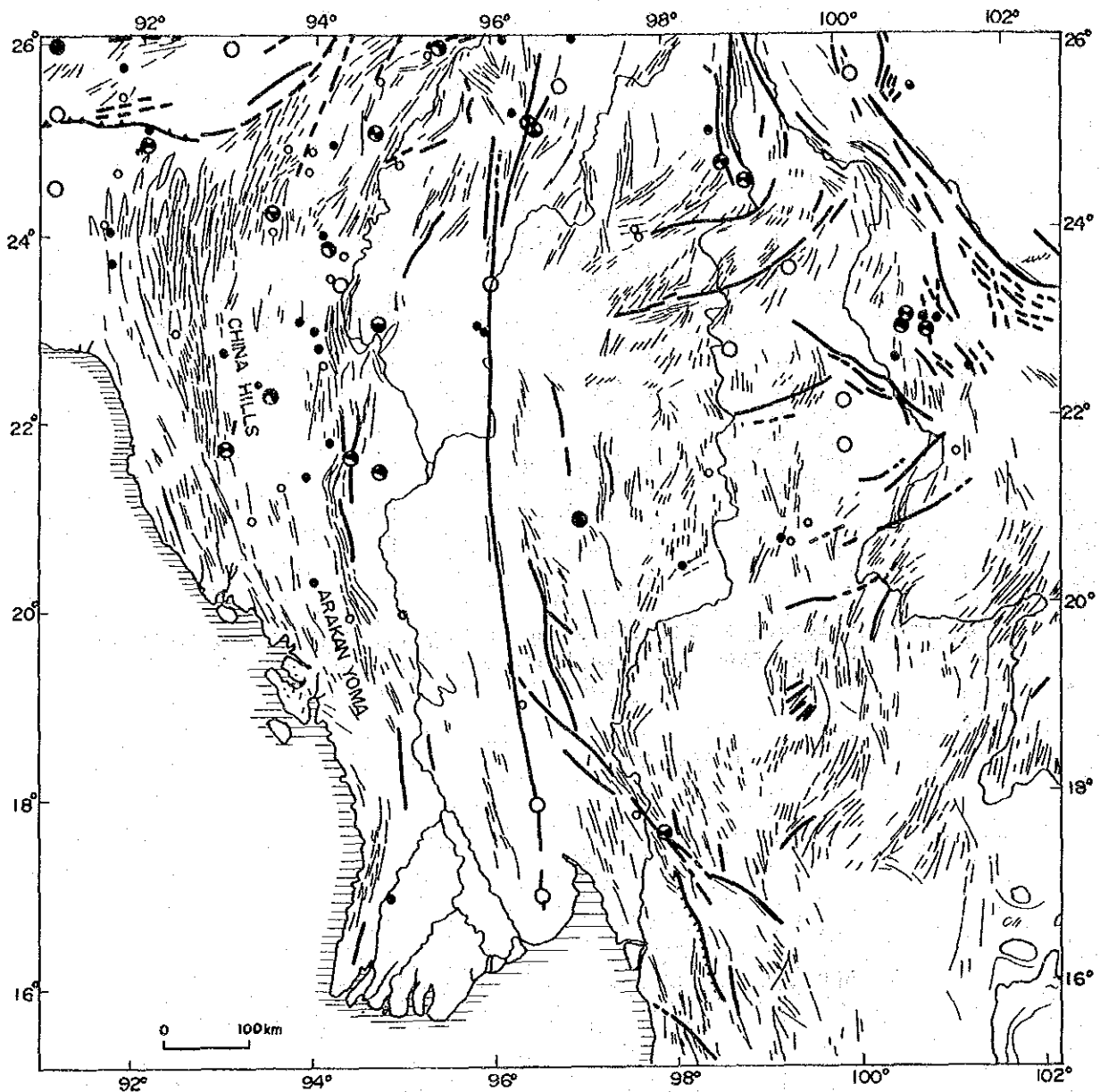


Fig. 7-20 Seismotectonic Map of Thailand and the Adjoining Regions
 JOURNAL OF GEOPHYSICAL RESEARCH, VOL. 89, NO. B1, PAGES 453-472, JANUARY 10, 1984

The Sagaing strike-slip fault, between Pegu and Mandalaya, is a particularly outstanding active tectonic feature. Bold lines are major active faults; thin lines, less important faults; dashed lines, ancient or inferred faults; dotted lines, bedding trends in sedimentary rocks or occasionally trends of elongated topographic ridges. For lower hemisphere projections of fault plane solutions, shaded and dotted areas are quadrants with compressional first motions for shallow and intermediate earthquakes, respectively, and white areas are quadrants with dilatations. Large solid and open circles correspond to historic events with $M > 7.8$ and $7.0 < M < 7.8$, respectively; for other shallow events, solid circles represent locations with more than 25 stations with residuals less than 1 second and with at least two such stations in each quadrant, and open circles are those with more than 15 stations with residuals less than 1 s and with at least one such station in each quadrant. Corresponding locations for intermediate earthquakes are shown by circles with crosses and circles with dots. Elevations are in meters.

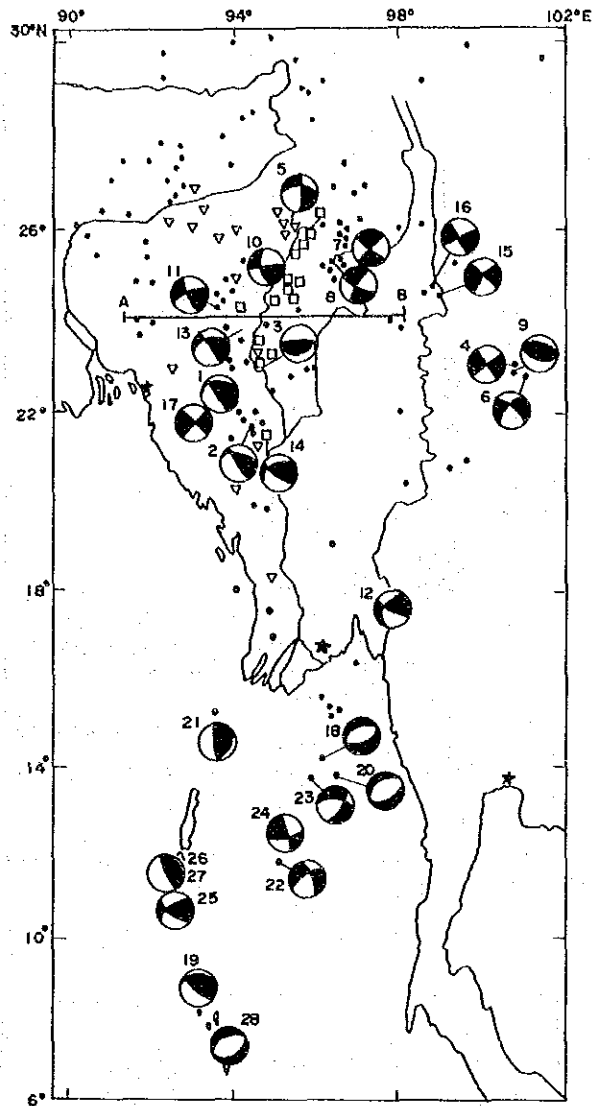


Fig. 7-21 Seismicity Map around Mae Lama Luang Damsite
 The epicenters have been plotted with symbols corresponding to depth (z) intervals: dark circles, $0 < z < 45$ km; triangles, $45 < z < 100$ km; squares, $100 < z < 150$ km. Symbols for fault plane solutions are the same as in Fig. 7-20.

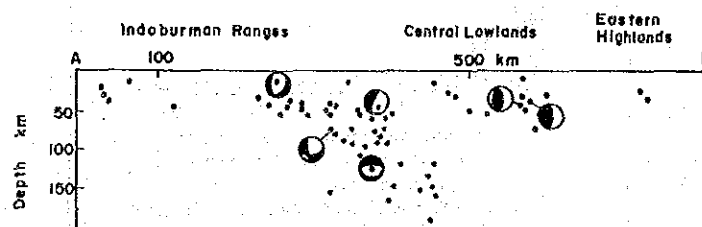


Fig. 7-22 Projections of the Locations of Earthquakes and Fault Plane Solutions onto the Plane A-B in Figure 7-21. Fault Plane solutions are plotted as back hemisphere projections. Symbols are the same as in Fig. 7-21.

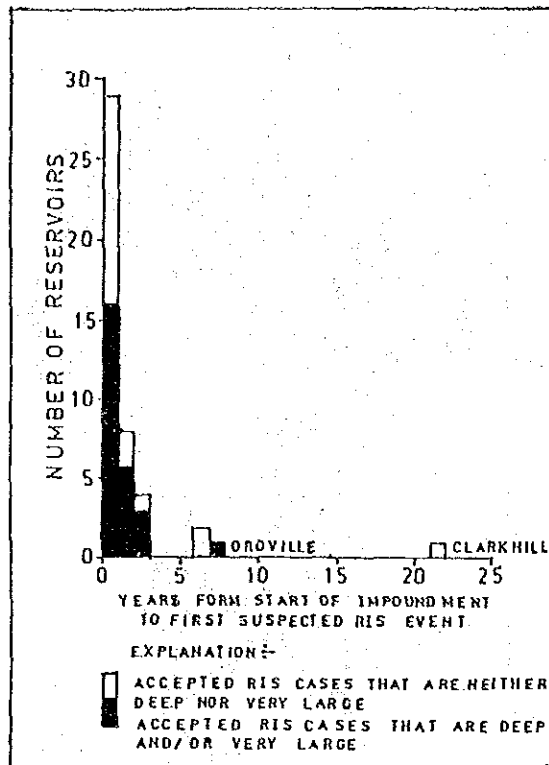


Fig. 7-23 'Time Lag' between Impoundment and First RIS Event (Packer et al, 1979).

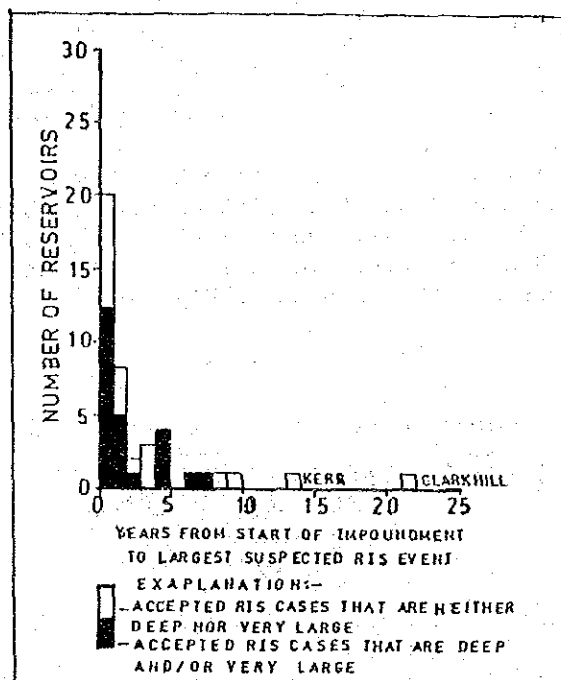


Fig. 7-24 'Time Lag' between Impoundment and Larger RIS Event (Packer et al, 1979).

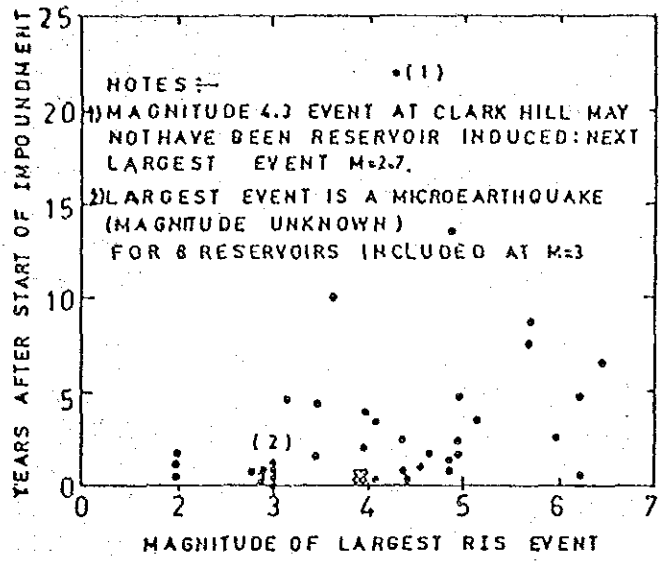


Fig. 7-25 Magnitude of the Largest RIS Event Versus 'Time Lag' of accepted Cases of RIS (Packer et al, 1979).

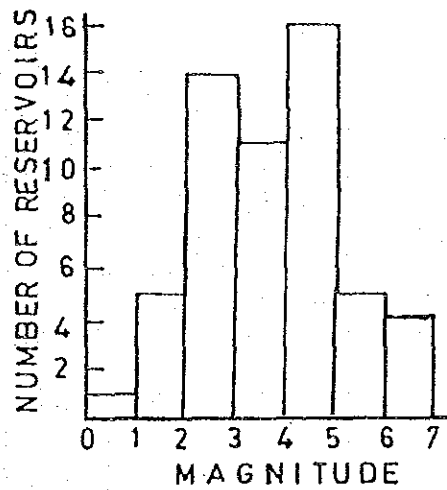


Fig. 7-26 Magnitudewise Distribution of reported RIS Cases. (after Guha, S. K.)

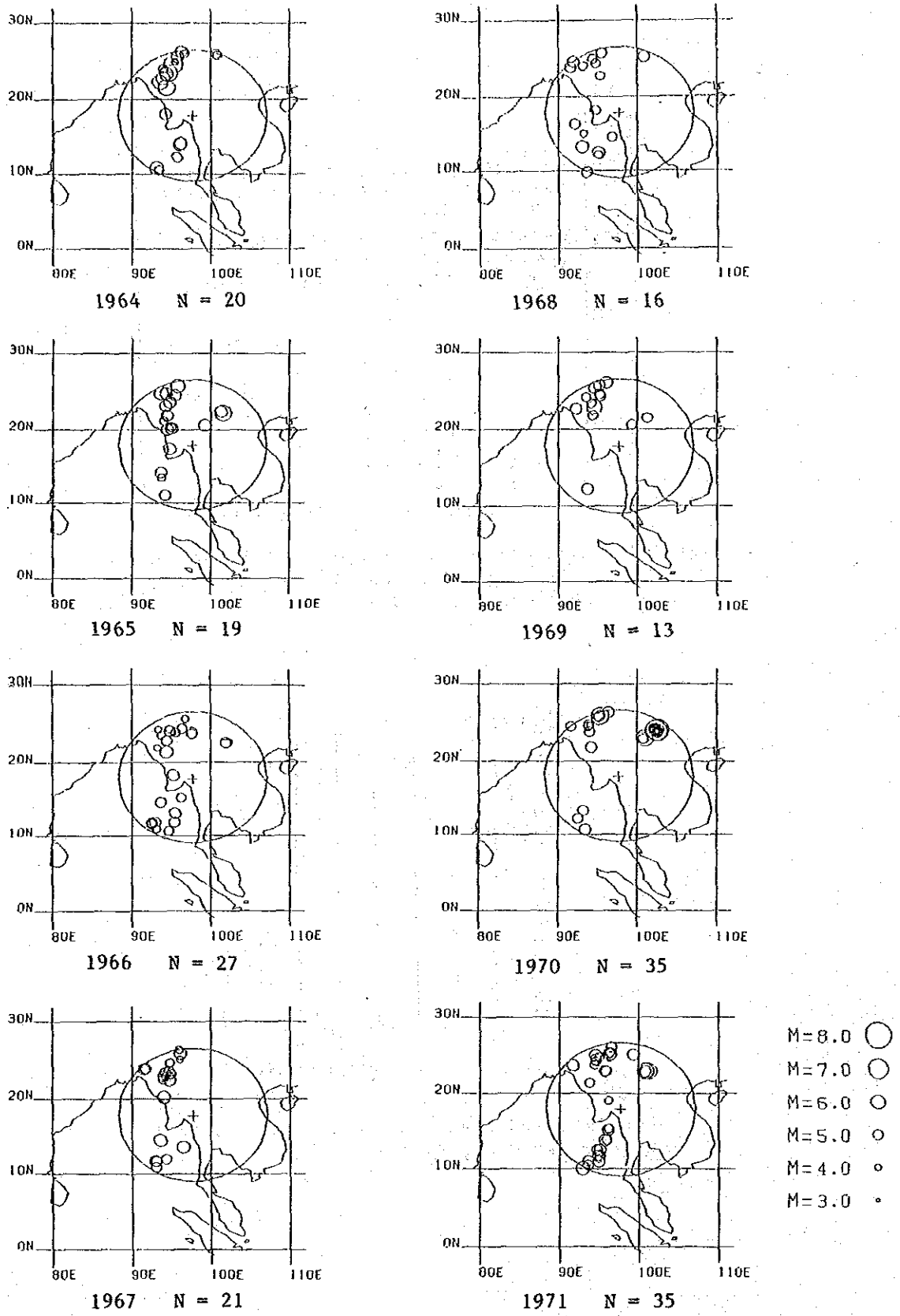


Fig. 7-27 Annual Distribution of the Earthquakes ($M \geq 3.0$) within 1,000 km in Radius from Mae Lama Luang Damsite (1964 - 1971)

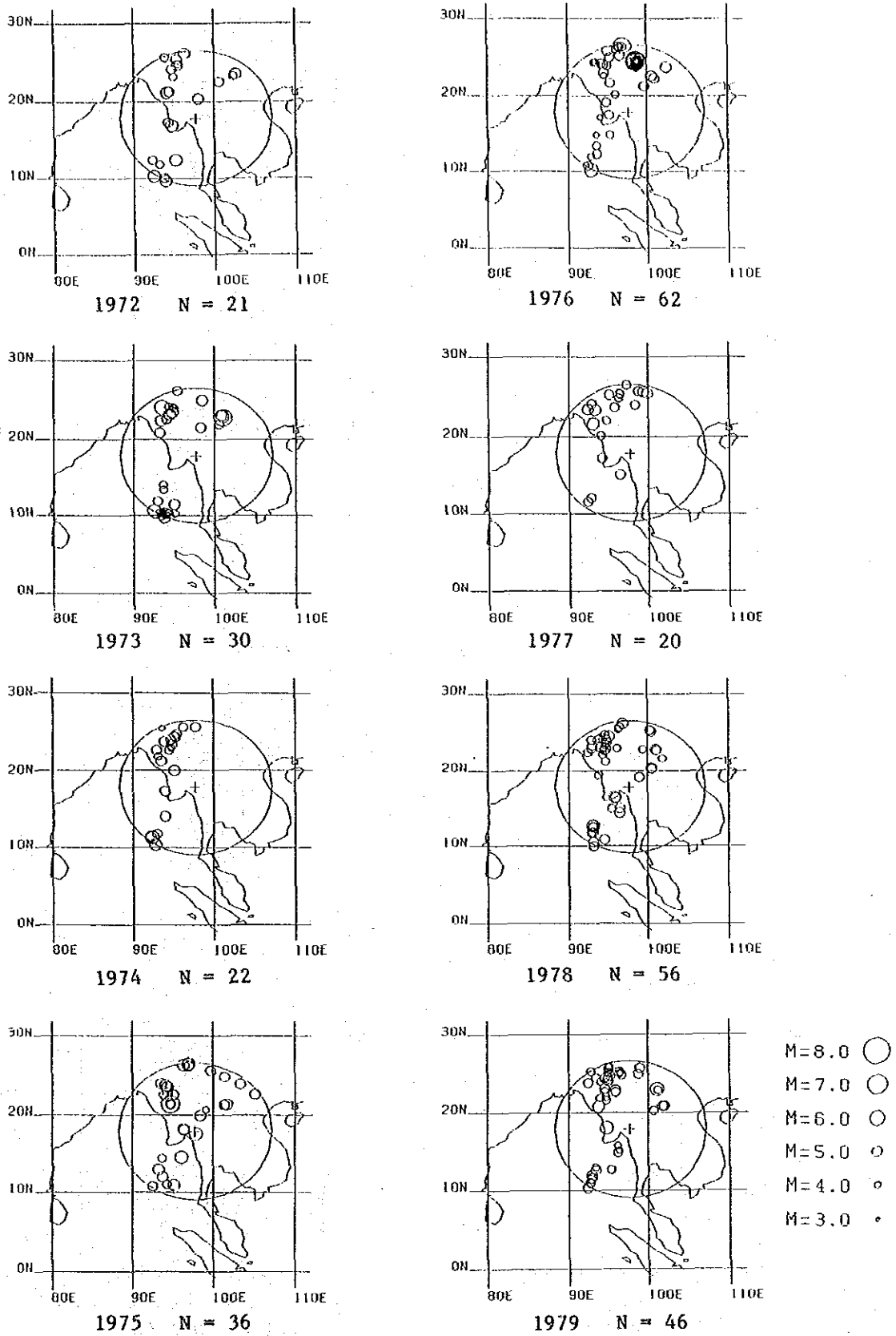


Fig. 7-28 Annual Distribution of the Earthquakes ($M \geq 3.0$) within 1,000 km in Radius from Mae Lama Luang Damsite (1972 - 1979)

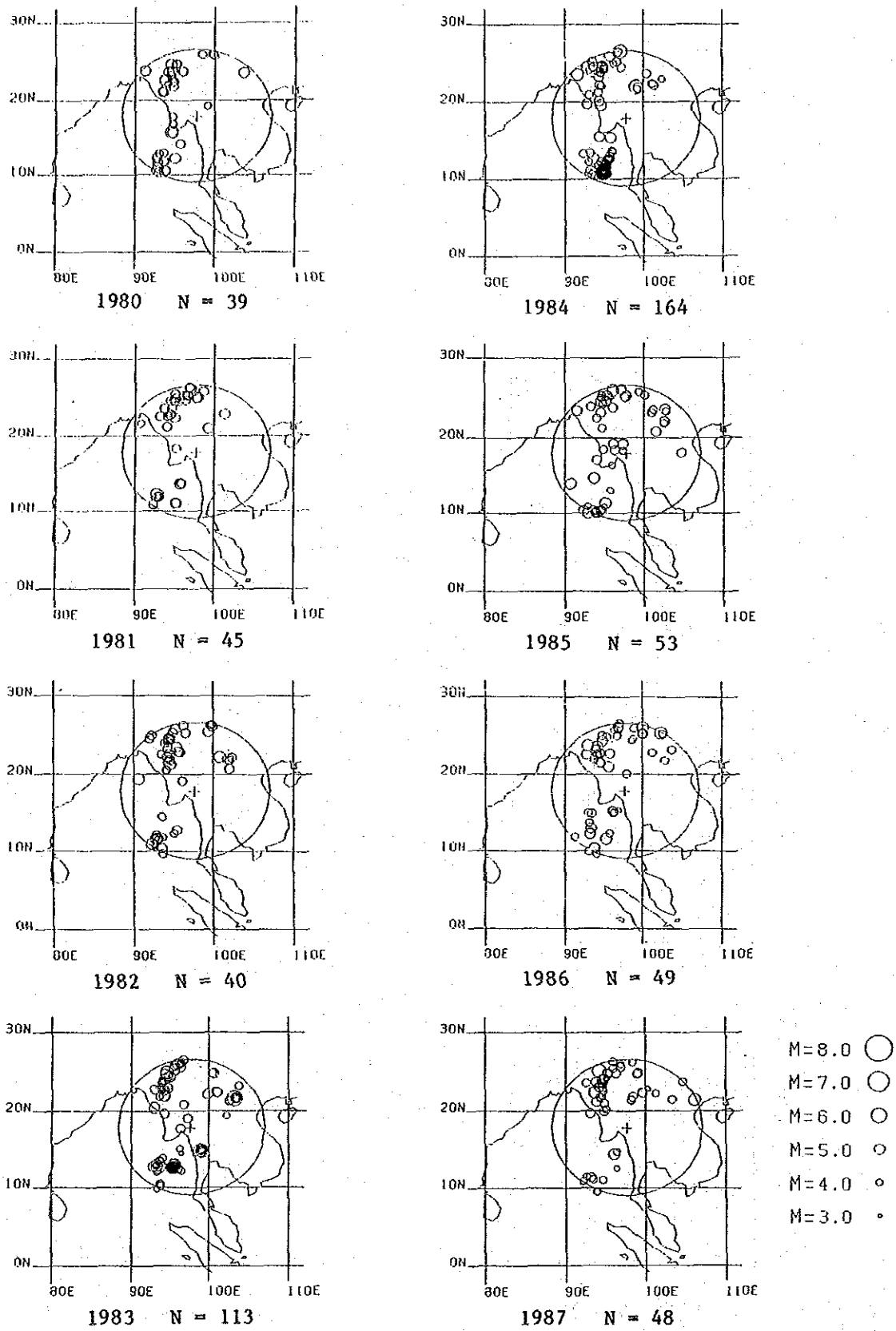


Fig. 7-29 Annual Distribution of the Earthquakes ($M \geq 3.0$) within 1,000 km in Radius from Mae Lama Luang Damsite (1980 - 1987)

7.4 Seismic Risk Analysis

7.4.1 Estimation of Maximum Acceleration

(1) Seismicity Data

Seismicity data used in this study are based on those retrieved from "The Earthquake Data File" released from National Geophysical Data Center, National Oceanic and Atmospheric Administration, United States Department of Commerce. Regarding earthquake events having their epicenters within 1,000 km in radius from the project site, total number compiled in the file is 1,107 during the period from 1901 to 1987. However, the number before 1958 is only 42.

Taking the attenuation characteristics of the peak amplitude of the earthquake ground motion into account, it can be judged that the range of 1,000 km in radius from the site is enough for estimation.

The locations of all the earthquake events after 1901 are plotted in Fig. 7-30, in which the project area (17°47'N, 97°48'E) is shown by the cross. Numbers of the events in each year during the period are shown in Table 7-4.

General features of the events such as magnitudes and epicentral distances from the site can be seen in Table 7-5.

(2) Attenuation Models

Of previously proposed attenuation models which express peak ground acceleration A (gal), in terms of earthquake magnitude M , and hypocentral distance R (km), or epicentral distance D (km), the following four models are used in this study.

$$\text{Log } A = 3.090 + 0.347 M = 2 \text{ Log } (R + 25) \quad (1)$$

proposed by C. Oliveira

$$\text{Log } A = 2.674 + 0.278 M - 1.301 \text{ Log } (R + 25) \quad (2)$$

proposed by R. K. McGuire

$$\text{Log } A = 2.041 + 0.347 M - 1.6 \text{ Log } R \quad (3)$$

proposed by L. Esteva and E. Rosenblueth

$$\text{Log } A = 2.308 + 0.411 M - 1.637 \text{ Log } (R + 30) \quad (4)$$

proposed by T. Katayama

For all the events, the values of peak acceleration were calculated by using the above attenuation models. As a result, annual maximum accelerations during the period were found as shown in Table 7-6.

In Table 7-6, the acceleration for 1975 derived from Eq. (2) is the largest of all. The earthquake event related to this acceleration has the magnitude 5.6 with the epicentral distance of 19 km and the depth of 6 km.

(3) Gumbel's Extreme Value Theory

If the probability variable : x obeys the probability function $G(x)$,

$$G(x) = Q(X \leq x)$$

The probability that x is larger than each of X_1, X_2, \dots, X_n is defined by:

$$P_n(x) = Q(X_1 \leq x, X_2 \leq x, \dots, X_n \leq x) = G_n(x)$$

And, the return period : $T(x)$ and the transform variable Z are expressed by the following equation.

$$T(x) = 1 / \{ 1 - P_n(x) \}$$

$$Z = -\ln \{ -\ln P_n(x) \}$$

Use of Gumbel's theory (1958) does not require knowledge of the parent distribution. When applied to deal with the seismological problems, it gives the estimates of the frequency of occurrence of events on the extreme of a statistical distribution, and also given an estimate of recurrent times for these

events, if the following main conditions involved in the development of theory are met :

- 1) The conditions prevailing in the past will definitely be valid in the future.
- 2) The observed largest events in a given interval are independent.
- 3) The behaviour of the largest earthquake in a given interval in the future will be similar to that of the past.

According to Gumbel, there are three types of asymptotic distributions of extremes, each corresponding to a specific type of behavior of large values of the variable.

The first type asymptotic distribution

$$P_n(x) = \exp [- \exp (-\alpha n)(x - V)]$$

The second type asymptotic distribution

$$P_n(x) = \exp [- (V - \epsilon)/(x - \epsilon)^k]$$

The third type asymptotic distribution

$$P_n(x) = \exp [- (W - x)/(W - V)^k]$$

In the first type asymptotic distribution, the variable is unlimited. The second type introduces a lower limit for the variable. And the third type introduces an upper limit. In this study, a probability function of the maximum acceleration expected at the project site is not known. However, it is reasonable to suppose that the function should be associated with the third type asymptotic distribution, because the maximum amplitude of earthquake ground motion for the arbitrary site should have an upper limit.

In the equation for the third type asymptotic distribution, W is an upper limit of a variable, k is a shape parameter, V is a characteristic value, and x is a random variable taken as logarithm of the maximum acceleration during a year-long interval, express as:

$$x = \log A_{\max}$$

Plotting position of the ordered series is calculated by:

$$p(m) = (N - m + 1) / (N + 1)$$

where, N is the total years of record, and m is the order of the value from the largest one.

(4) Statistical Analysis Results

The seismicity data are used for 29 years from 1959 to 1987. Hence, a probabilistic model based on the "Gumbel's Extreme Values Theory" can be established by setting an equal time interval to one year.

Although a probability function of the maximum acceleration at the project site is not known, it is reasonable to suppose that the function should be associated with the third type asymptotic distribution.

The previously mentioned maximum acceleration values are plotted in Fig. 7-31 to Fig. 7-34. In these figures, two kinds of regression curves estimated for the third asymptotic distribution function are also shown by solid lines, from which the maximum acceleration for any return period can be evaluated.

The curve "B" is a result evaluated by method of least squares for all the annual maximum acceleration points, and regression curve "A" is a result evaluated to cross the annual maximum acceleration point of 1975.

Table 7-7 shows the maximum accelerations expected at the site for different four return periods of 50, 100, 200 and 500 years.

According to the results of the statistical analysis based on the earthquake data from 1958 to 1987, the maximum acceleration by McGuire's equation are very large compared with the other equations, i.e. Oliveira's equation, Esteva & Rosenblueth's equation and Katayama's equation.

The result for long return period by McGuire's equation, shown in Fig. 7-32, is mainly governed by the annual maximum acceleration of 1975 (120.67 gal).

As shown in Fig. 7-31 to Fig. 7-34, the points for annual maximum acceleration of 1975 are distributed discontinuously. As an engineering judgement, it is considered that the analysis results by regression curve [A] are not necessarily reasonable, but safer.

7.4.2 Seismic Risk Map for Thailand

It is necessary to execute the seismic analysis for the arbitrary sites, in order to draw up the seismic risk map. In the study introduced here, the seismic risk analysis based on Gumbel's Extreme Value Theory was made by applying the third type asymptotic distribution. The maximum amplitude of earthquake ground motion was estimated for all the points by every one degree in both latitude and longitude, in the region between 0° - 24° N of latitude and 93° - 111° E of longitude. The seismicity data was selected from NOAA earthquake data file.

Earthquake events which occurred between 5° S and 35° N of latitude and 85° - 125° E of longitude during the years 1901 to 1977 were used in the seismic risk analysis. As for the events whose focal depths are undecided, the focal depth is assumed to be 20 km. And as for undecided magnitude, the following assumption is made.

Year	Assumed Magnitude
1901 - 1950	M 6.0
1951 - 1960	M 5.0
1961 - 1977	M 4.0

And, two kinds of attenuation model shown below are used.

(1) Kanai's Equation

Kanai's Equation is proposed for evaluating the maximum velocity of earthquake motion at the rock surface. Kanai's attenuation model is very popular and often used in Japan.

(2) Oliveira - McGuire's Equation

This equation gives the maximum acceleration at ground surface without considering the ground characteristics. A-line in Fig. 7-35 shows the results by Oliveira - McGuire's Equation.

Kanai's Equation

$$\log V = 0.61M - \left(1.66 + \frac{3.60}{D}\right) \log D - (0.631 + 1.83/D) \quad (5)$$

Oliveira - McGuire Average Equation

$$\log A = 2.882 + 0.313M - 1.651 (R + 25) \quad (6)$$

here, V : Maximum Velocity (kine)

A : Maximum Acceleration (gal)

R : Hypocentral Distance (km)

D : Epicentral Distance (km)

[for reference]

Oliveira's Equation

$$\log A = 3.090 + 0.347M - 2 \log (R + 25) \quad (7)$$

McGuire's Equation

$$\log A = 2.674 + 0.278M - 1.301 \log (R + 25) \quad (8)$$

As a whole, Oliveira-McGuire's equation gives an average estimate of various attenuation models proposed in the world.

The estimated maximum velocity contour maps regarding Thailand and the adjoining regions for different three return periods of 50, 100,

and 200 years are shown in Fig. 7-36, Fig. 7-37, Fig. 7-38, respectively. The maximum velocities of 0.5, 1, 2, 5, 10, 15, 20, 30 and 45 kine are contoured in these figures.

Similarly, the estimated maximum acceleration contour maps for return periods of 50, 100, and 200 years are shown in Fig. 7-39, Fig. 7-40, Fig. 7-41, respectively. The maximum accelerations of 20, 50, 100, 150, 200, 250, 300, 400 and 500 gal are contoured.

Taking the maximum velocity distribution and the maximum acceleration distribution described above into consideration, seismic risk map for Thailand and the adjoining regions are made, which is shown in Fig. 7-42.

Estimated values of maximum velocity and maximum acceleration for return period of 200 years at the project site can be considered to be 2 - 5 kine and 50 - 100 gal, respectively. The project site is located in the seismic risk zone "D" in the seismic risk map.

Table 7-4 Number of Earthquakes in a Year
during the Period from 1901 to 1987

Year	N	Sum of N	Year	N	Sum of N
1901	1	1	1945	0	25
1902	0	1	1946	0	25
1903	0	1	1947	0	25
1904	0	1	1948	1	26
1905	0	1	1949	0	26
1906	0	1	1950	3	29
1907	0	1	1951	1	30
1908	1	2	1952	1	31
1909	1	3	1953	0	31
1910	0	3	1954	1	32
1911	0	3	1955	4	36
1912	0	3	1956	4	40
1913	1	4	1957	2	42
1914	1	5	1958	0	42
1915	0	5	1959	1	43
1916	0	5	1960	1	44
1917	0	5	1961	6	50
1918	0	5	1962	3	53
1919	0	5	1963	14	67
1920	0	5	1964	20	87
1921	0	5	1965	19	106
1922	0	5	1966	27	133
1923	1	6	1967	21	154
1924	0	6	1968	16	170
1925	2	8	1969	13	183
1926	0	8	1970	35	218
1927	0	8	1971	35	253
1928	0	8	1972	21	274
1929	2	10	1973	30	304
1930	5	15	1974	22	326
1931	1	16	1975	36	362
1932	0	16	1976	62	424
1933	1	17	1977	20	444
1934	2	19	1978	56	500
1935	0	19	1979	46	546
1936	0	19	1980	39	585
1937	0	19	1981	45	630
1938	1	20	1982	49	679
1939	0	20	1983	113	792
1940	1	21	1984	165	957
1941	3	24	1985	53	1,010
1942	1	25	1986	49	1,059
1943	0	25	1987	48	1,107
1944	0	25			

Table 7-5 Distribution of Magnitude and Epicentral Distance of the Seismicity Data

	0 < M < 3.5	< 4.0	< 4.5	< 5.0	< 5.5	< 6.0	< 6.5	< 7.0	< 7.5	< 8.0	< 8.5	Total
< 100	0	0	1	0	0	0	0	0	0	0	0	1
< 200	0	0	0	3	3	0	0	0	0	0	0	6
< 300	0	1	5	5	4	1	0	0	0	0	0	16
< 400	1	2	12	17	14	5	0	0	0	0	0	51
< 500	0	0	9	16	8	7	0	2	0	0	0	42
< 600	0	2	22	46	22	2	1	4	0	0	0	99
< 700	1	4	46	77	41	6	9	4	0	0	0	188
< 800	1	4	31	84	51	13	6	2	1	0	0	193
≤ 1,000	0	5	27	72	49	45	22	6	1	1	0	228
Total	1	0	153	320	192	80	38	18	2	1	0	825

: Epicentral Distance (km)
M : Magnitude

Table 7-6 Maximum Annual Acceleration during
a Year from 1959 to 1987

Year	Oliveira, C. Eq. (1)	McGuire, R.K. Eq. (2)	Esteva, L. & Rosenblueth, E. Eq. (3)	Katayama, T. Eq. (4)
1959	0.22	3.53	0.30	0.99
1960	0.19	3.32	0.28	0.95
1961	0.27	3.97	0.35	1.11
1962	0.40	5.43	0.52	1.78
1963	0.22	3.62	0.31	1.06
1964	0.58	6.98	0.71	2.46
1965	0.77	7.44	0.80	2.29
1966	0.93	8.31	0.93	2.58
1967	0.44	5.32	0.51	1.55
1968	0.50	5.29	0.52	1.39
1969	0.44	4.95	0.48	1.30
1970	0.55	7.52	0.77	3.10
1971	0.72	6.64	0.69	2.00
1972	0.72	7.12	0.75	2.17
1973	0.46	6.04	0.59	2.07
1974	0.45	5.09	0.49	1.36
1975	53.77	120.67	80.38	67.52
1976	0.67	6.34	0.67	1.71
1977	0.53	5.53	0.55	1.47
1978	1.38	11.02	1.35	3.78
1979	0.90	8.42	0.93	2.75
1980	0.57	6.21	8.63	1.86
1981	0.47	4.86	0.48	1.18
1982	0.67	6.13	0.65	1.57
1983	2.24	13.86	1.99	4.48
1984	0.59	6.09	0.62	1.92
1985	2.75	14.74	2.41	4.36
1986	0.56	5.86	0.59	1.63
1987	0.42	4.89	0.47	1.32

Table 7-7 Maximum Accelerations Expected at the Project Site
for 4 Return Periods (gal)

Attenuation Model	Return Period (Year)			
	50	100	200	500
(1) by C. Oliveira	56.0	57.2	57.8	58.0
(2) by R.K. McGuire	123.2	124.4	124.8	125.1
(3) by Est. & Rosen.	82.5	83.4	83.7	83.8
(4) by T. Katayama	69.3	70.1	70.4	70.5

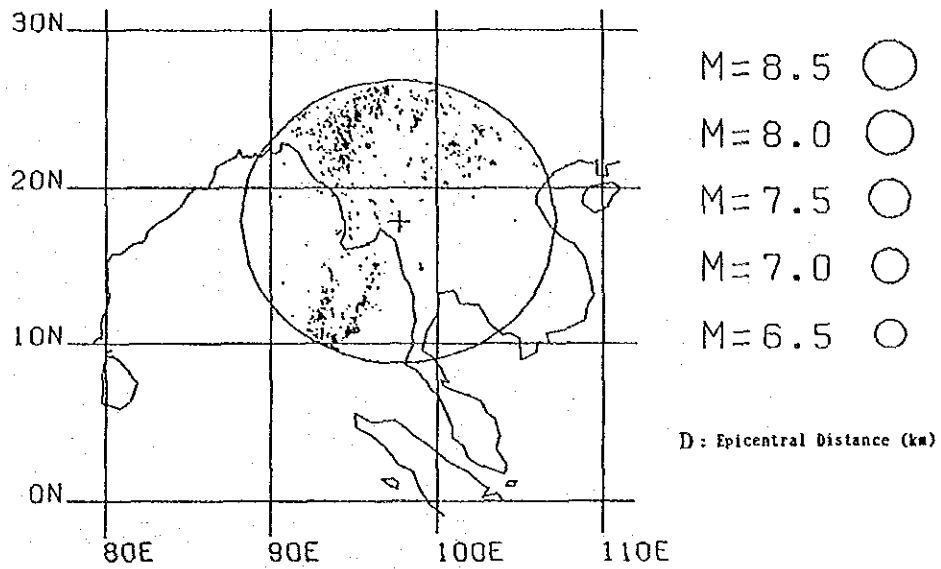


Fig. 7-30 Seismicity of All Data in 1901 - 1987
 Total number of plots in the area of $D \leq 1,000$ km is 1,107

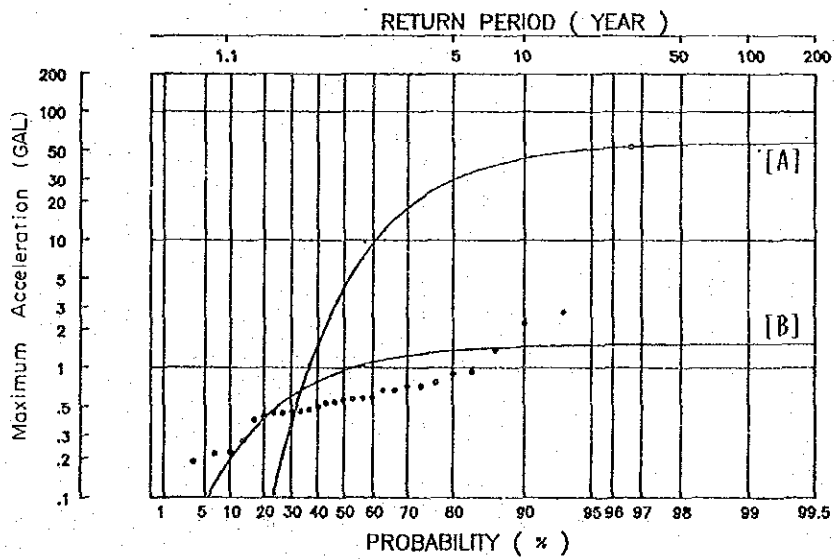


Fig. 7-31 Return Period for Maximum Acceleration Estimated by Eq.-(1) [Oliveira]

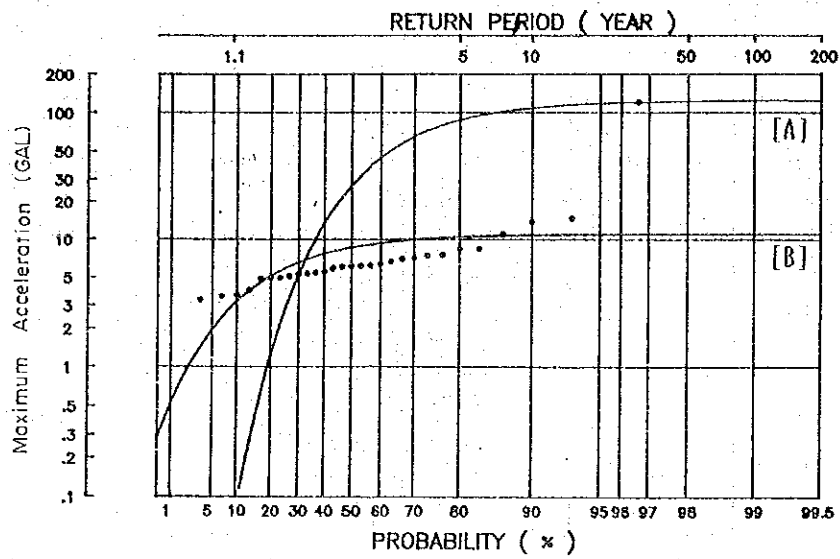


Fig. 7-32 Return Period for Maximum Acceleration Estimated by Eq.-(2) [McGuire]

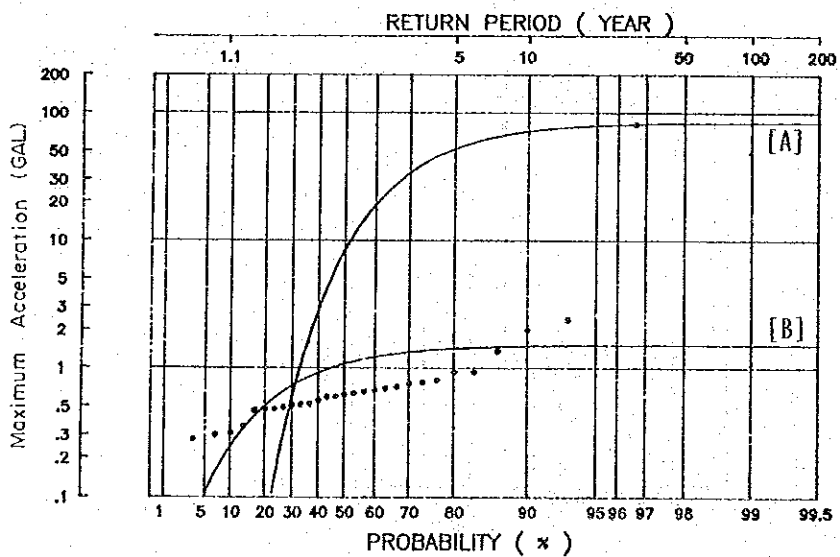


Fig. 7-33 Return period for Maximum Acceleration Estimated by Eq.-(3) [Esteva & Rosenblueth]

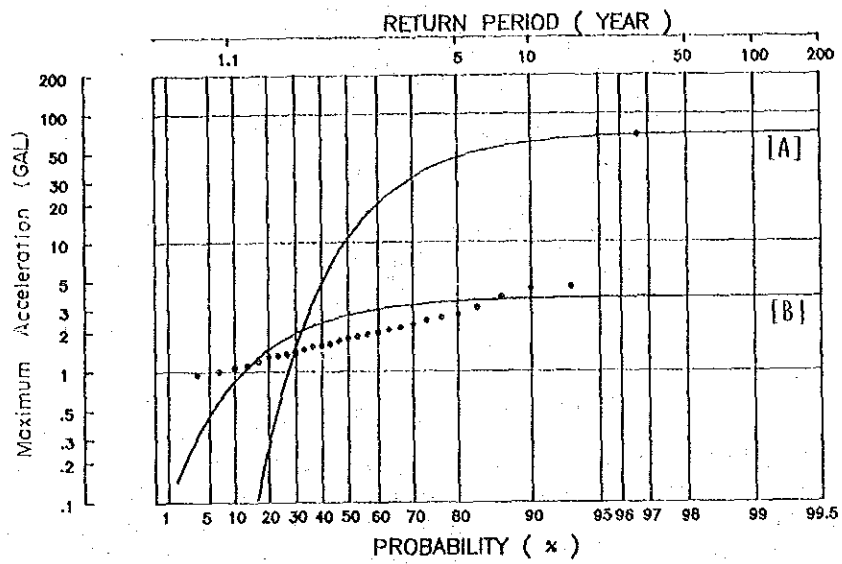


Fig. 7-34 Return Period for Maximum Acceleration Estimated by Eq.-(4) [Katayama]

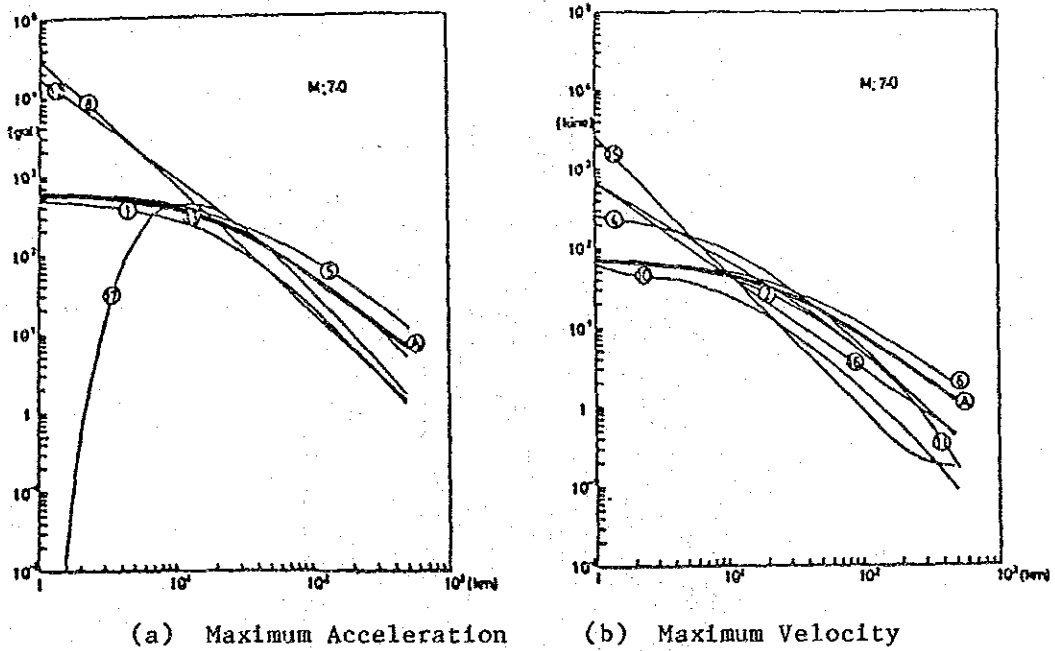


Fig. 7-35 Comparisons of Various Attenuation Models (M = 7.0)

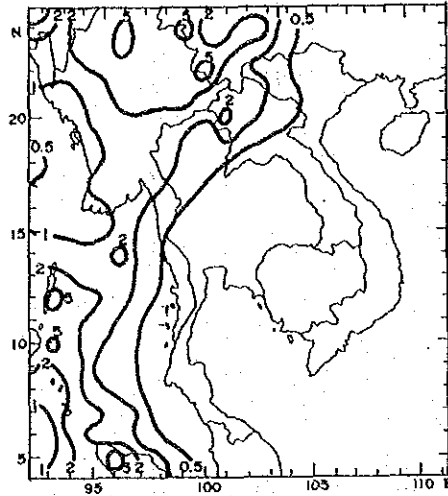


Fig. 7-36 Regional Distributions of the Maximum Earthquake Motion in and around Thailand. V_{max} for Return Period $T_r = 50$ years. V_{max} (Kine): Maximum particle velocity on the base rock. A_{max} (gal) : Maximum acceleration on the ground)

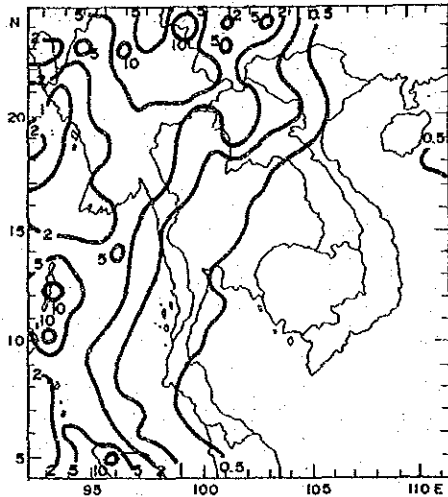


Fig. 7-37 Seismic Risk Map in and around Thailand V_{max} for Return Period $T_r = 100$ Years.

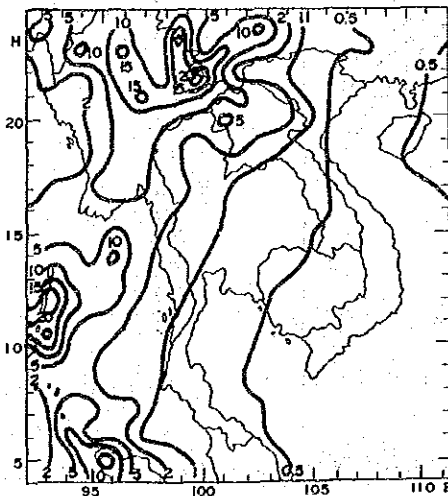


Fig. 7-38 Seismic Risk Map in and around Thailand V_{max} for Return Period $T_r = 200$ Years.

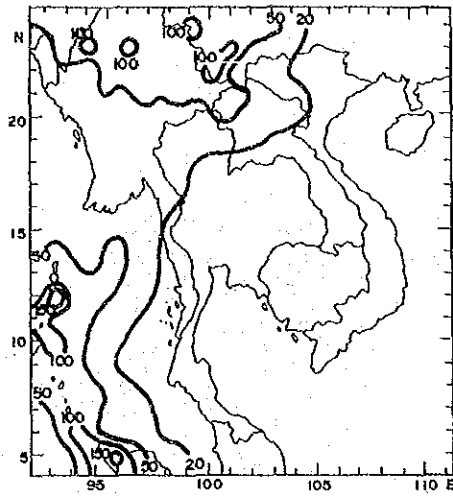


Fig. 7-39 Seismic Risk Map in and around Thailand
Amax for Return Period $T_r = 50$ years.

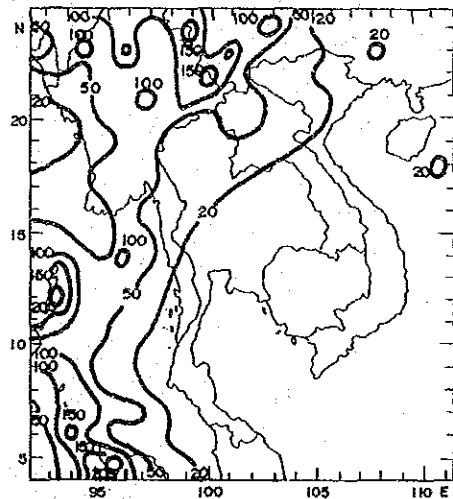


Fig. 7-40 Seismic Risk Map in and around Thailand
Amax for Return Period $T_r = 100$ Years.

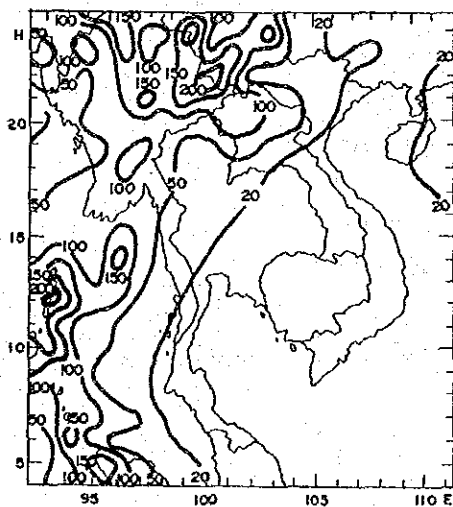


Fig. 7-41 Seismic Risk Map in and around Thailand
Amax for Return Period $T_r = 200$ Years.

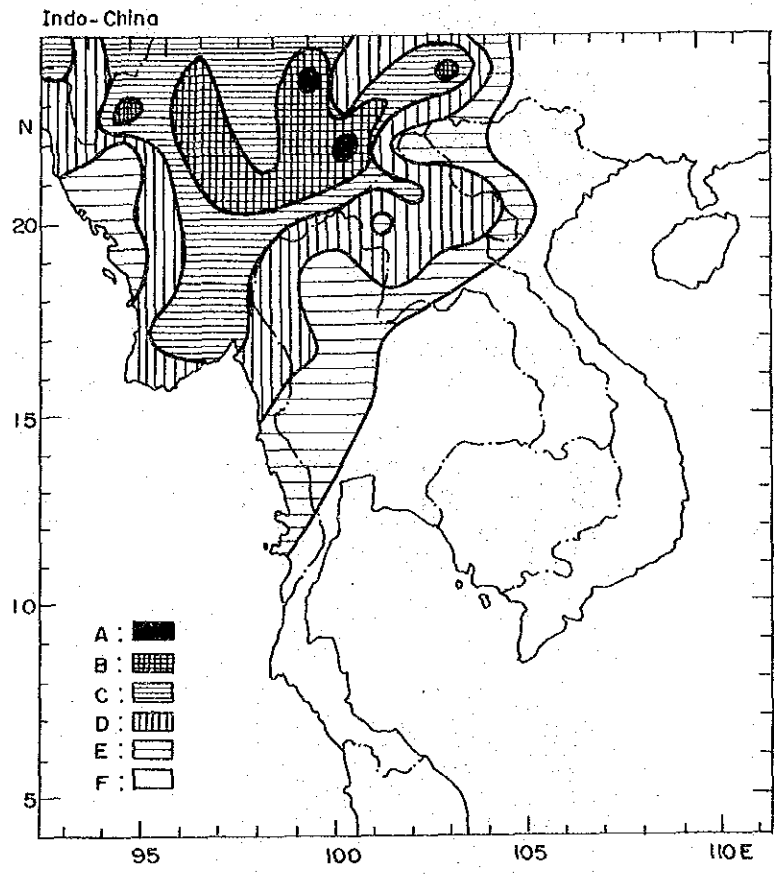


Fig. 7-42 Seismic Zoning Map for Thailand and the Adjacent Regions

- A : 1st degree
- B : 2nd degree
- C : 3rd degree
- D : 4th degree
- E : 5th degree
- F : no danger

Seismic zones are divided based on V_{max} value.

7.5 Seismic Coefficient for the Project Site

The estimated values of the maximum acceleration at the project area is summarized in Table 7-8.

There is no well-established theory about the relationship between the maximum acceleration of the earthquake motion and the value of the design seismic coefficient. However, it is possible to list up some methods to convert the maximum acceleration of the earthquake motion into the design seismic coefficient, as described below.

Method-(1) : The method to divide A_{max} by 980 simply and directly.

The Simplest Method.

$$= A_{max}/980$$

: Design seismic coefficient

A_{max} : Maximum acceleration of the motion (gal)

Method-(2) : The method to calculate the effective design seismic coefficient. Empirical Method.

eff: Effective design seismic coefficient

R : Reduction factor (Empirical Value of R is
approximately 0.5 - 0.65)

Method-(3) : The method to evaluate the equivalent design seismic coefficient by executing the dynamic analysis with dynamic model. The most reasonable method at present.

Method-(1) is the simplest method to convert the maximum acceleration into the seismic coefficient. However, this method evaluates rather large value of seismic coefficient compared with "the real value". Generally speaking, the longer the predominant period of earthquake motion, the larger the stresses produced inside the dam for the same maximum acceleration of the earthquake motion. The static analysis method is a method to evaluate the stresses and deformations by inputting the static inertia force to the analysis model as an earthquake force. In other words, the static analysis method can be considered as a kind of dynamic analysis method with inputting the harmonic wave of period $T = \infty$ as a design input motion, or, the earthquake force. Therefore, Method-(1) will often overestimates the design seismic coefficient.

Method-(2) was proposed based on empirical knowledges at first. However, the similar results are reported in the recent studies on the dynamic analysis and the static analysis. Method-(2) can be considered to be more available method in comparison with Method-(1).

Method-(3) is the most reasonable method at present. However, Method-(3) cannot be available, unless the design input motion, the soil-structure model, the properties of the rock materials, etc. are known.

Taking into consideration the above, it is decided to apply Method-(2) in this study for estimating the seismic coefficient from the maximum acceleration.

It can be concluded that the design horizontal seismic coefficient of 0.10 for the Mae Lama Luang and Nam Ngao dams was adopted, according to the estimated maximum accelerations.

Table 7-8 Estimates of Maximum Acceleration at
Nam Yuam Project Area

[Annual Maximum Acceleration]									
Year	Location	Epicenter		M	R (km)	Estimates of Maximum Acceleration at the Site (gal)			
		LAT (°N)	LONG (°E)			Eq.- (1)	Eq.- (2)	Eq.- (3)	Eq.- (4)
1975	Near Field	17.638	97.902	5.6	20	53.77	120.67	80.38	67.52
[Statistical Analysis Result]									
Return Period (year)		Probability (%)			Eq.- (1)	Eq.- (2)	Eq.- (3)	Eq.- (4)	
50		98			56.0	123.2	82.5	69.3	
100		99			57.2	124.4	83.4	70.1	
200		99.5			57.8	124.8	83.7	70.4	
500		99.9			58.0	125.1	83.8	70.5	

- R : Hypocentral Distance (km)
- D : Epicentral Distance (km)
- Eq.-(1) : proposed by C. Oliveira
- Eq.-(2) : proposed by R. K. McGuire
- Eq.-(3) : proposed by L. Esteva and E. Rosenblueth
- Eq.-(4) : proposed by T. Katayama

Table 7-9 Estimated Value of Design Seismic Coefficient based on the Maximum Accelerations

Estimated Value	Basis for Estimation
R = 0.65	<p>The estimated maximum acceleration by the statistical analysis is controlled by the near field earthquake.</p> <p>Near Field Earthquake → Excell in High Frequency → High Reduction 0.65 is the empirical value, which is often used.</p>
Amax = 125 (gal)	<p>Maximum Acceleration by Attenuation Model 120.67 (gal) 1975 by Eq.-(2) Statistical Analysis Result 125.1 (gal): Eq.-(2)</p>
eff = 0.10	<p>eff = R.Amax/980 → 0.10</p>

CHAPTER 8

DEVELOPMENT PLAN

CHAPTER 8 DEVELOPMENT PLAN

CONTENTS

	<u>Page</u>
8.1 Methodology and Basic Conditions of Study	8 - 1
8.1.1 Methodology	8 - 1
8.1.2 Basic Conditions	8 - 6
8.2 Selection of Dam Sites	8 - 14
8.2.1 Nam Ngao Project	8 - 14
8.2.2 Mae Lama Luang Project	8 - 16
8.3 Optimization Study on Individual Development	8 - 35
8.3.1 Nam Ngao Project	8 - 35
8.3.2 Mae Lama Luang Project	8 - 38
8.4 Optimization Study on Integrated Development	8 - 56
8.5 Finalization of Selected Development Plans	8 - 78
8.5.1 Selected Development Plan of Investigation Stage	8 - 78
8.5.2 Finalization of the Projects	8 - 79
8.6 Study on Sequence of Projects' Implementation and Adopted Development Plan	8 - 92
8.6.1 Alternatives of Projects' Implementation	8 - 92
8.6.2 Adopted Development Plan and Implementation	8 - 94

List of Tables

- Table 8-1 Topographical and Geological Comparison of Alternative Dam Sites of Nam Ngao Project
- Table 8-2 Economic Comparison Study on Nam Ngao Dam Site
- Table 8-3 Topographical and Geological Comparison of Alternative Dam Sites of Mae Lama Luang Project
- Table 8-4 Economic Comparison Study on Mae Lama Luang Dam Site
- Table 8-5 Study on NHWL and Effective Storage Capacity of Nam Ngao Project (Individual Development)
- Table 8-6 Study on Maximum Power Discharge of Nam Ngao Project (Individual Development)
- Table 8-7 Study on NHWL and Effective Storage Capacity of Mae Lama Luang Project (Individual Development)
- Table 8-8 Study on Maximum Power Discharge of Mae Lama Luang Project (Individual Development)
- Table 8-9 Study on NHWL and Effective Storage Capacity of Nam Ngao and Mae Lama Luang Projects (Integrated Development)
- Table 8-10 Study on Maximum Power Discharge of Nam Ngao and Mae Lama Luang Projects (Integrated Development)
- Table 8-11 Finalized Development Plan (Individual Development)
- Table 8-12 Finalized Development Plan (Integrated Development)
- Table 8-13 Study on Sequence of Projects' Implementation
- Table 8-14 Monthly List of Power
- Table 8-15 Monthly List of Energy

List of Figures

- Fig. 8-1 Location of Dam Sites
- Fig. 8-2 Reservoir Area and Storage Capacity Curve of Nam Ngao Project (Site No. 2)
- Fig. 8-3 Reservoir Area and Storage Capacity Curve of Mae Lama Luang Project (Site No. 4 and No. 5)
- Fig. 8-4 Rating Curves of Nam Ngao Project
- Fig. 8-5 Rating Curves of Mae Lama Luang Project
- Fig. 8-6 Mass Curve of Nam Ngao Project
- Fig. 8-7 Study on NHWL and Effective Storage Capacity of Nam Ngao Project (Individual Development)
- Fig. 8-8 Study on Maximum Power Discharge of Nam Ngao Project (Individual Development)
- Fig. 8-9 Mass Curve of Mae Lama Luang Project (Individual Development)
- Fig. 8-10 Study on NHWL and Effective Storage Capacity of Mae Lama Luang Project (Individual Development)
- Fig. 8-11 Location of Villages and the Number of Households to be Resettled
- Fig. 8-12 Study on Maximum Power Discharge of Mae Lama Luang Project (Individual Development)
- Fig. 8-13 Mass Curve of Mae Lama Luang Project (Integrated Development)
- Fig. 8-14 Study on NHWL and Effective Storage Capacity of Nam Ngao and Mae Lama Luang Project (Integrated Development)
- Fig. 8-15 Study on Maximum Power Discharge of Nam Ngao and Mae Lama Luang Project (Integrated Development)
- Fig. 8-16 Reservoir Operation Rule Curves
- Fig. 8-17 Reservoir Operation of Nam Ngao Project
- Fig. 8-18 Reservoir Operation of Mae Lama Luang Project (Individual Development)
- Fig. 8-19 Reservoir Operation of Mae Lama Luang Project (Integrated Development)
- Fig. 8-20 Flow Diagram for the Calculation of Energy Production
- Fig. 8-21 Alternatives of Projects' Implementation

List of Drawings

- DWG. 8-1 Comparison of Dam Site
General Plan
Nam Ngao Dam Site No. 1
- DWG. 8-2 Comparison of Dam Site
General Plan
Nam Ngao Dam Site No. 2
- DWG. 8-3 Comparison of Dam Site
General Plan
Nam Ngao Dam Site No. 3
- DWG. 8-4 Comparison of Dam Site
General Plan
Mae Lama Luang Dam Site No. 4
- DWG. 8-5 Comparison of Dam Site
General Plan
Mae Lama Luang Dam Site No. 5
- DWG. 8-6 Comparison of Dam Site
General Plan
Mae Lama Luang Dam Site NEA

CHAPTER 8 DEVELOPMENT PLAN

8.1 Methodology and Basic Conditions of Study

8.1.1 Methodology

The main objective of this chapter is to determine the development scale of the Nam Ngao project and the Mae Lama Luang project. Since the projects are located near to each other, the one project affects the other project for determining their development scale such as dam height, installed capacity, etc. Considering the above, the development scale of both projects are determined on the basis of the methodology mentioned below.

(1) Stages of Study

The study consists of the following two stages.

- Investigation Stage

Alternative dam sites for the Nam Ngao project and the Mae Lama Luang project are evaluated, and the most suitable sites are selected for both projects. Then, optimization study is carried out on the selected dam sites of both projects. The optimum project scales of the projects are determined for an individual development and for an integrated development.

- Feasibility Design Stage

Taking into account the result of the study of the Investigation Stage and up-to-date data of the geology, flood discharge, etc., both projects are studied in more detail. Then, the projects' development scale is finalized.

(2) Selection of Dam Site and Optimization Study

- Selection of Dam Site (Investigation Stage)

As shown in Fig. 8-1, three alternative dam sites for the Nam Ngao project and three sites for the Mae Lama Luang project are compared from topographical, geological and economic points of view. The most suitable site is selected for each project.

- Optimization Study (Investigation Stage)

After determining the dam sites for the Nam Ngao and the Mae Lama Luang projects, the optimization study varying the normal high water level (NHWL), effective storage and maximum power discharge is done. The study consists of the following cases.

◦ Individual Development Plan

Nam Ngao Project (Individual)

Mae Lama Luang Project (Individual)

◦ Integrated Development Plan

Overall plan taking into account both Nam Ngao and Mae Lama Luang projects

- Finalization of Selected Development Plan
(Feasibility Design Stage)

The development scale of the Nam Ngao project and the Mae Lama Luang project is finalized for individual development and integrated development, taking into account the most up-to-date information as follows;

◦ electric power demand and supply forecast (plant factor)

◦ geology and construction materials

◦ design flood

- design of structures (including transmission line)
 - reservoir operation
 - compensation and resettlement
- Determination of Development Periods and Sequence
(Feasibility Design Stage)

Their development sequence, development scale at each stage, and the timing of extension of the Mae Lama Luang power plant are considered.

In determining the development sequence, a priority is given to a project which shows better economy and can be separated from related projects in consideration of the power supply plan. Also considered will be the cost for installing power transmission lines, which governs the economy of the project.

(3) Reservoir Operation and Energy Production

- Reservoir Operation

The 95% firm discharge is first obtained in order to study reservoir operation and to optimize the development scale.

(Investigation Stage)

The mass curve of runoff is drawn and the firm discharge for each year is obtained from the mass curve, on the assumption that past actual runoff is reproduced exactly in the same way and that the figures are completely foreseeable. The 95% firm discharge is obtained from a probability distribution of the firm discharge of each year under the most effective operation of the reservoir.

Evaporation loss is not considered for the reservoir operation study.

(Feasibility Design Stage)

The reservoir operation rule curve is constructed taking into account the 95% firm discharge. The rule curve can be applied for reservoir operation on the assumption that the runoff in the future is not foreseeable.

Evaporation loss is considered for the reservoir operation study.

- Equivalent Peak Duration Hours

The peak duration hours (plant factor) are closely related to load duration curves whose figure is mostly dependent on the power supply area.

Since the power supply area of the Nam Ngao and Mae Lama Luang projects is most reasonably considered to be the Northern region, the peak duration hours of 3.6 was determined based upon the daily load duration curve and daily load factor, etc. of the Northern region. The procedure how 3.6-hour is determined is described in Appendix.

- Maximum Power Discharge

In the study on selection of dam site, the discharge obtained by the 95% firm discharge and the equivalent peak duration hours is adopted as the maximum power discharge, tentatively. Then, the maximum power discharge is determined by the optimization study. This study is done in the investigation stage.

- Calculation of Energy Production

Energy production of each planned power station is calculated based on the monthly inflow for the 28 year period from 1959 to 1986 at each dam site.

The available head in each month for the energy calculation is derived from the reservoir water level, operated by the mass curve and the water level operated by the rule curve for

the investigation stage and the feasibility design stage, respectively.

- Firm Capacity

The output corresponding to an exceedance probability of 90% on the reservoir water level duration curve and peak discharge during equivalent peak duration hours is adopted as the firm capacity.

- Firm and Secondary Energy

(Investigation Stage)

The part of the annual energy production corresponding to the firm capacity is taken as the firm energy, and the energy production other than the firm energy is taken to be the secondary energy.

(Feasibility Design Stage)

The firm energy and secondary energy are not calculated. The reason is described in Chapter 12.

(4) Economic Comparison of Alternatives

(Investigation Stage)

Alternative plans are compared using the technique of the benefit-cost ratio (B/C) and annual surplus benefit (B-C). The cost (C) is the annual cost of hydro power project, and the benefit (B) is the annual cost of an alternative thermal power project having an serviceability equivalent to the hydro power project.

(Feasibility Design Stage)

The alternative plans and the sequence of the development of the projects are evaluated by using the Discounted Cash Flow method to calculate the Net Present Value (NPV) of B-C and the Equalizing Discount Rate (EDR)*. Since undeveloped hydro power resources in Thailand is reducing, NPV is attached impor-

tance in order to utilize the resources as much as possible. The detail of the methodology is described in Chapter 12 "Economic Justification".

(Note)* EDR is explained in Chapter 12.

8.1.2 Basic Conditions

(1) Topographical Maps

The six kinds of topographical maps listed below are available for the study.

Scale 1:250,000 whole river basin

Scale 1: 50,000 - ditto -

Scale 1: 10,000 Mae Lama Luang project area

Scale 1: 5,000 Nam Ngao project area,
a part of Mae Lama Luang project area

Scale 1: 1,000 Mae Lama Luang dam site (Site No.4 and No.5),
Nam Ngao dam site (Site No. 2)

Scale 1: 2,000 Mae Lama Luang dam site (Site NEA)

(2) Catchment Area and Reservoir Area - Storage Capacity Curve

- The catchment area of Nam Ngao project and Mae Lama Luang project was measured by EGAT, using 1:50,000 scale maps.

The Survey Team checked the catchment area of each projects prior to the Feasibility Study. The exactitude of the catchment area calculated by EGAT was confirmed and applied to the river flow calculation at the dam sites.

- Reservoir Area-Storage Capacity Curve

The maps of scale 1/5,000 and/or 1/10,000 are used for the reservoir area-storage capacity curves. However, as the maps do not cover a part of the project area of the Nam Ngao

reservoir, the maps of 1/50,000 are used for this part. The reservoir area-storage capacity curves for each site are shown in the following figures.

Nam Ngao project

Site No. 2 ... Fig. 8-2

Site No. 1 and No. 3 ... Appendix

Mae Lama Luang Project

Site No. 5 and No. 4 ... Fig. 8-3

Site NEA ... Appendix

- Preliminary Design

The maps of a scale of 1:1,000, 1:2,000 and 1:5,000 are used for the preliminary design.

(3) Rating Curves at the Powerhouse Site

- Nam Ngao project

(Site No. 1, No. 2)

The curve was drawn using backwater analysis from the confluence of the Yuam river and the Ngao river to Site No. 2. A coefficient of roughness of 0.035 is adopted for the analysis, and cross sections surveyed by EGAT were used. The rating curves for individual and integrated development are shown in Fig. 8-4.

(Site No. 3)

The difference between river bed elevation of the Site No. 2 and Site No. 3 was obtained from a 1:5,000 scale map, and the difference was added to the rating curve for Site No. 2.

- Mae Lama Luang project

(Site No. 4, No. 5, NEA)

The rating curve shown in Fig. 8-5 was made using backwater analysis from the confluence of the Moei river and the Yuam river to the Site NEA. The conditions for the analysis are the same as those for the Ngao project.

(4) Cost and Benefit of Projects

- Investigation Stage

The construction costs of alternative plans are estimated using the same unit cost used in the Master Plan, (July 1986), because significant change in the price level between July 1986 and the beginning of 1988 (start of the investigation stage) has not been confirmed.

The annual cost is calculated by multiplying the construction cost (without interest during construction and cost of transmission line) by the conversion factor (11.6%) of the annual cost.

The annual benefit is calculated based on the firm capacity, firm energy and secondary energy. The capacity value and the firm energy value are 1,810 $\text{\text{B}}$ /kW and 1.029 $\text{\text{B}}$ /kWh, respectively. The secondary energy value is 1.029 $\text{\text{B}}$ /kWh for the individual development plan and 0.967 $\text{\text{B}}$ /kWh for the integrated development plan. Further, these values were used in the Master Plan Study (See Master Plan Report page 9-16).

- Feasibility Design Stage

The economic comparison of alternatives is carried out with the method mentioned Chapter 12, and using up-to-date data concerning the construction costs of hydro plants, alternative thermal plants and fuel costs.

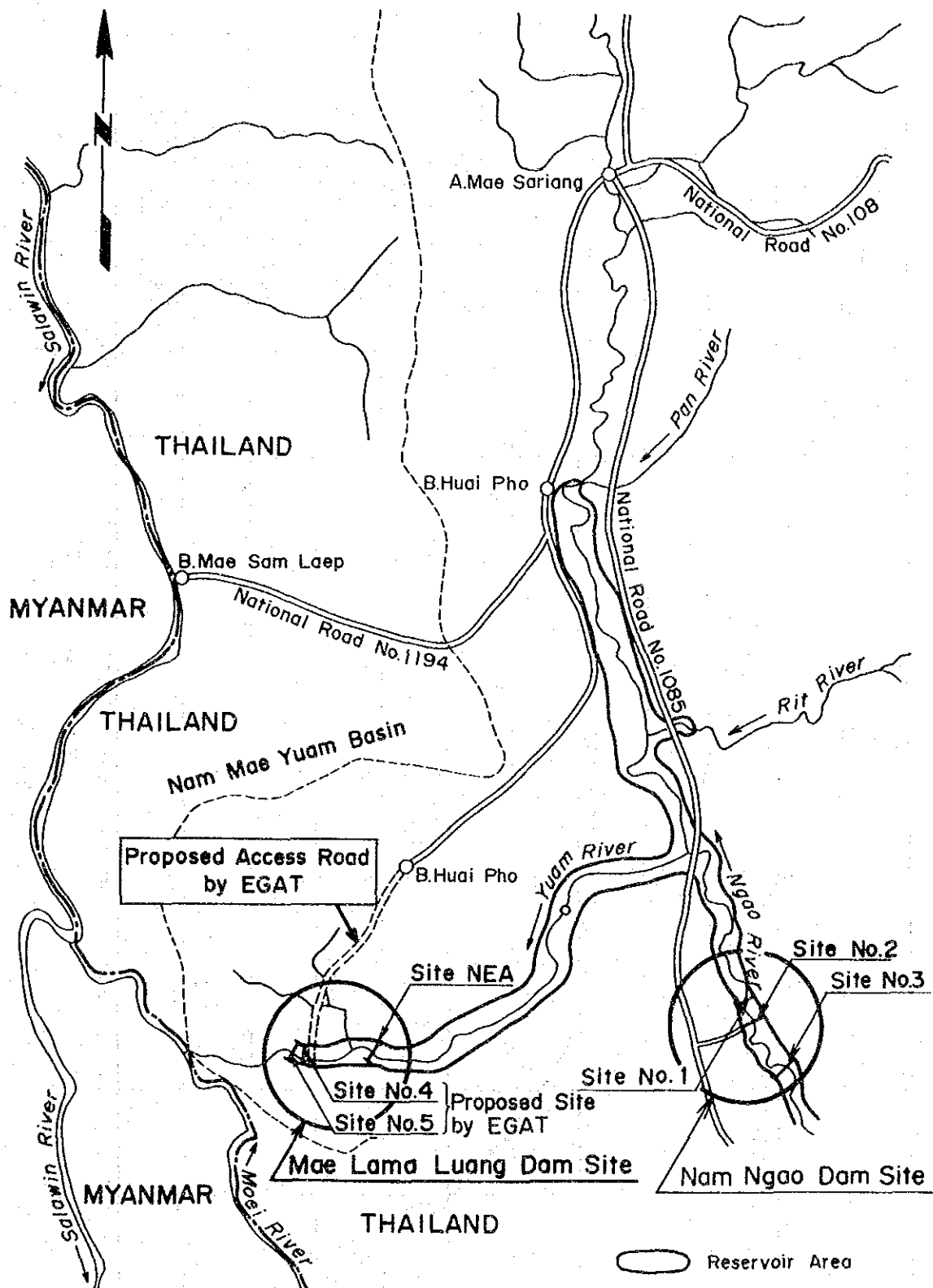


Fig.8-1 Location of Dam Sites

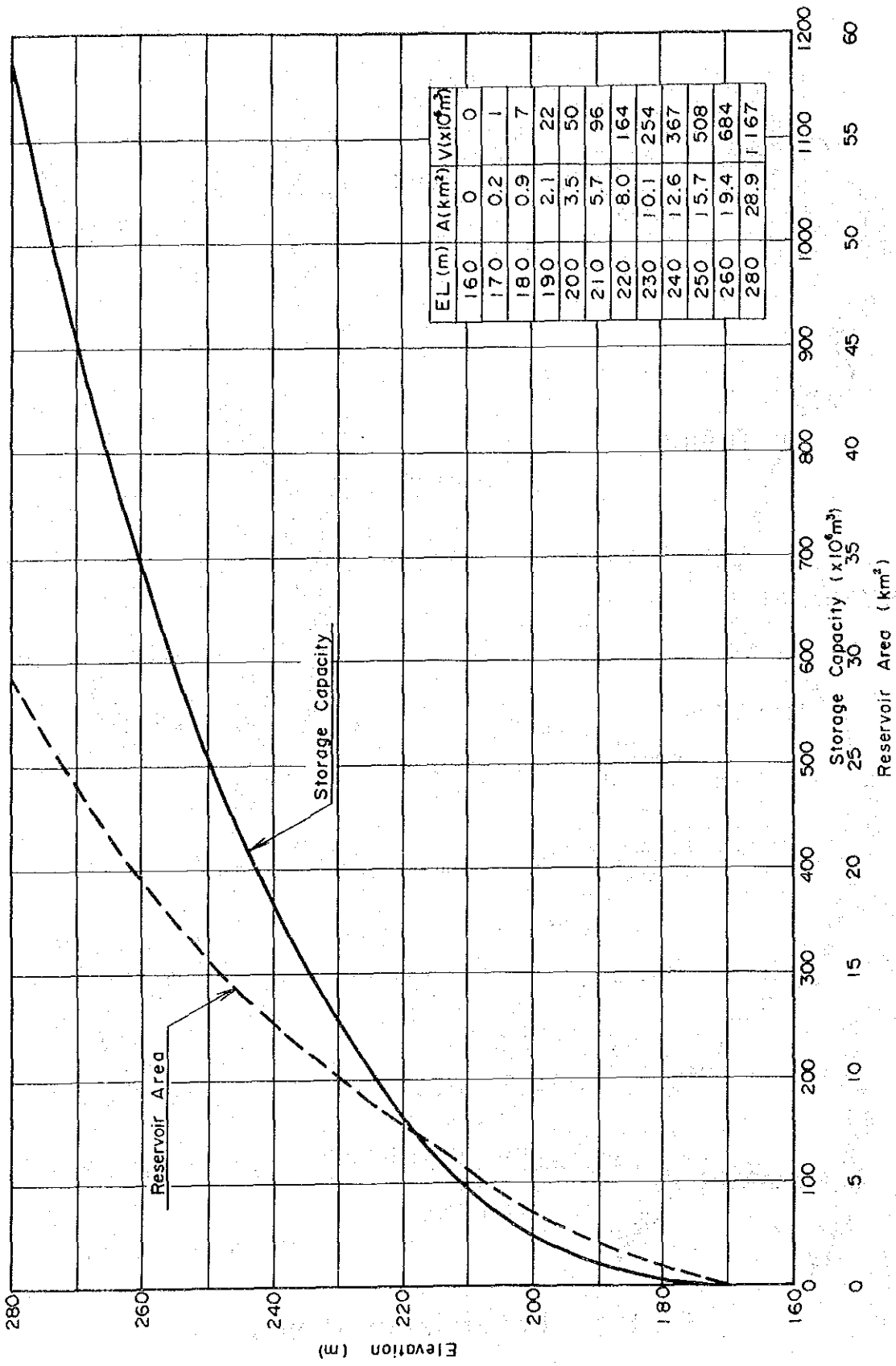


Fig. 8-2 Reservoir Area and Storage Capacity Curve of Nam Ngao Project (Site No.2)

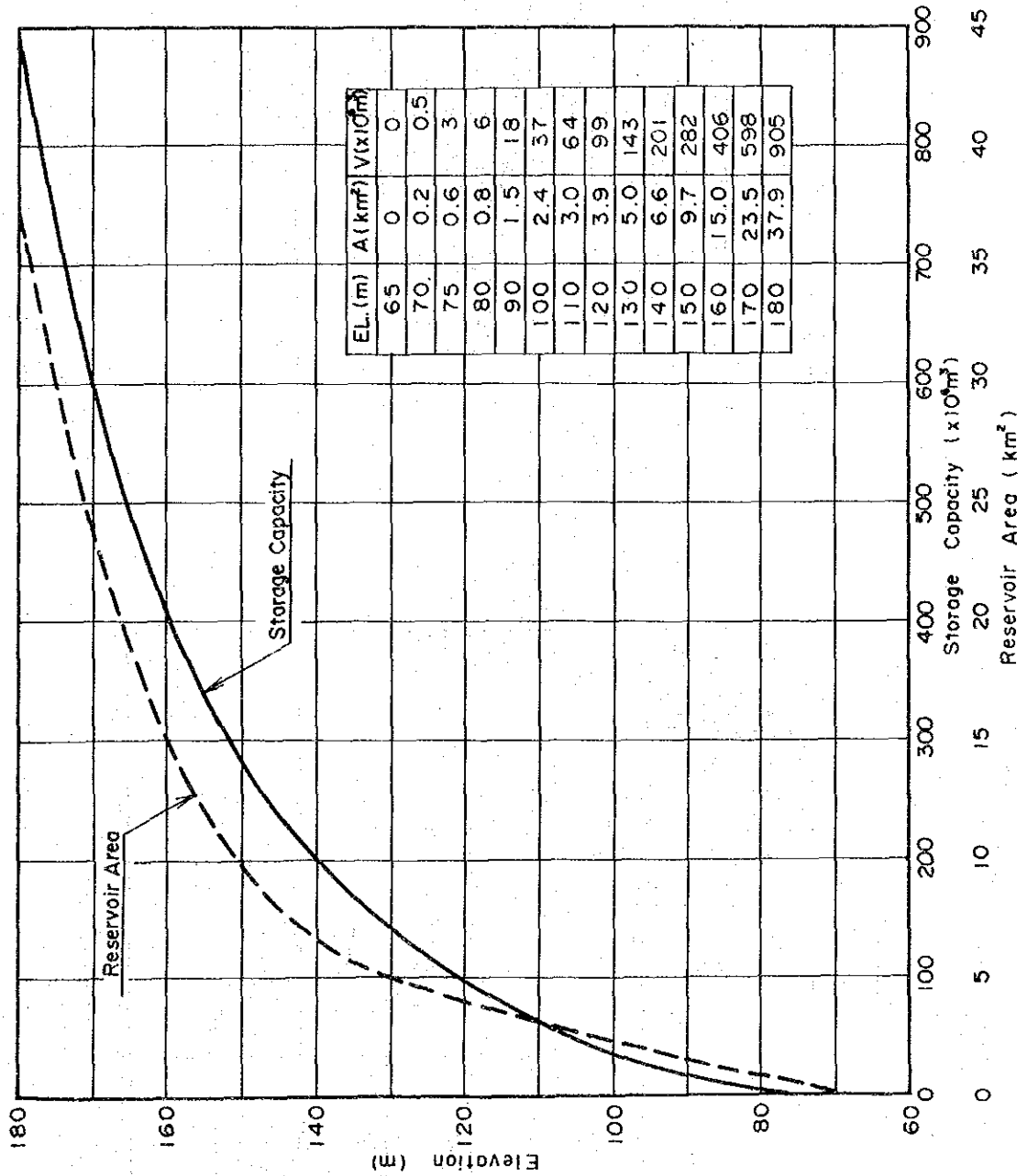


Fig. 8-3 Reservoir Area and Storage Capacity Curve of Mae Lama Luang Project (Site No.4 and No.5)

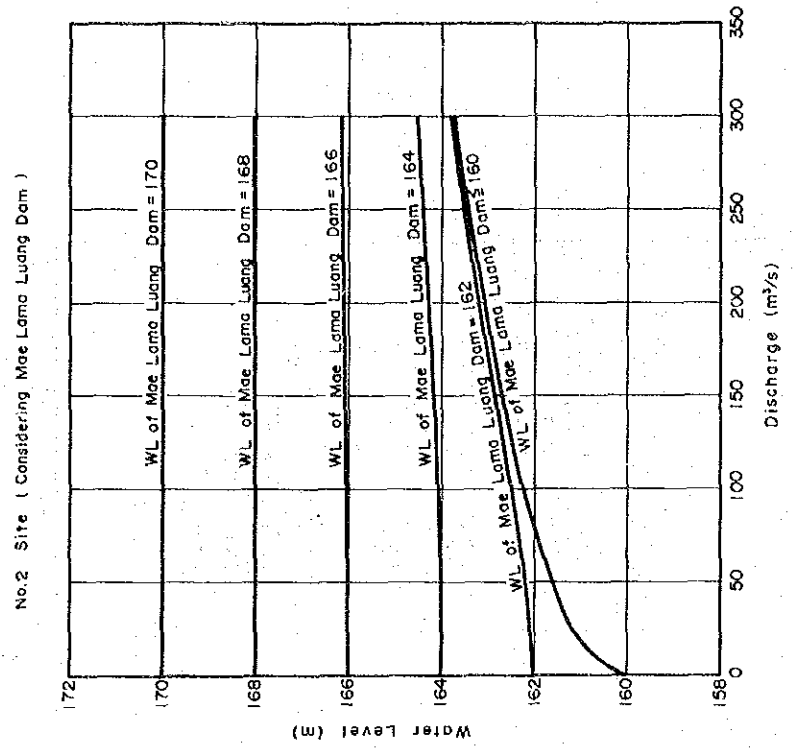
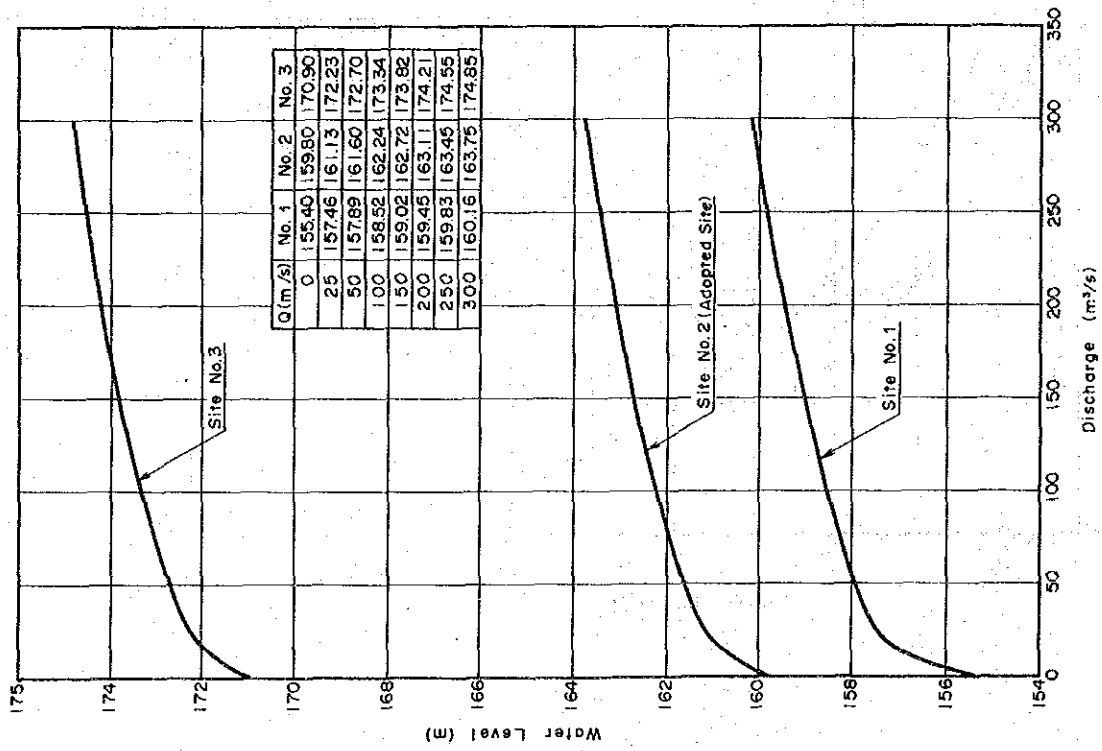


Fig. 8-4 Rating Curves of Nam Ngao Project

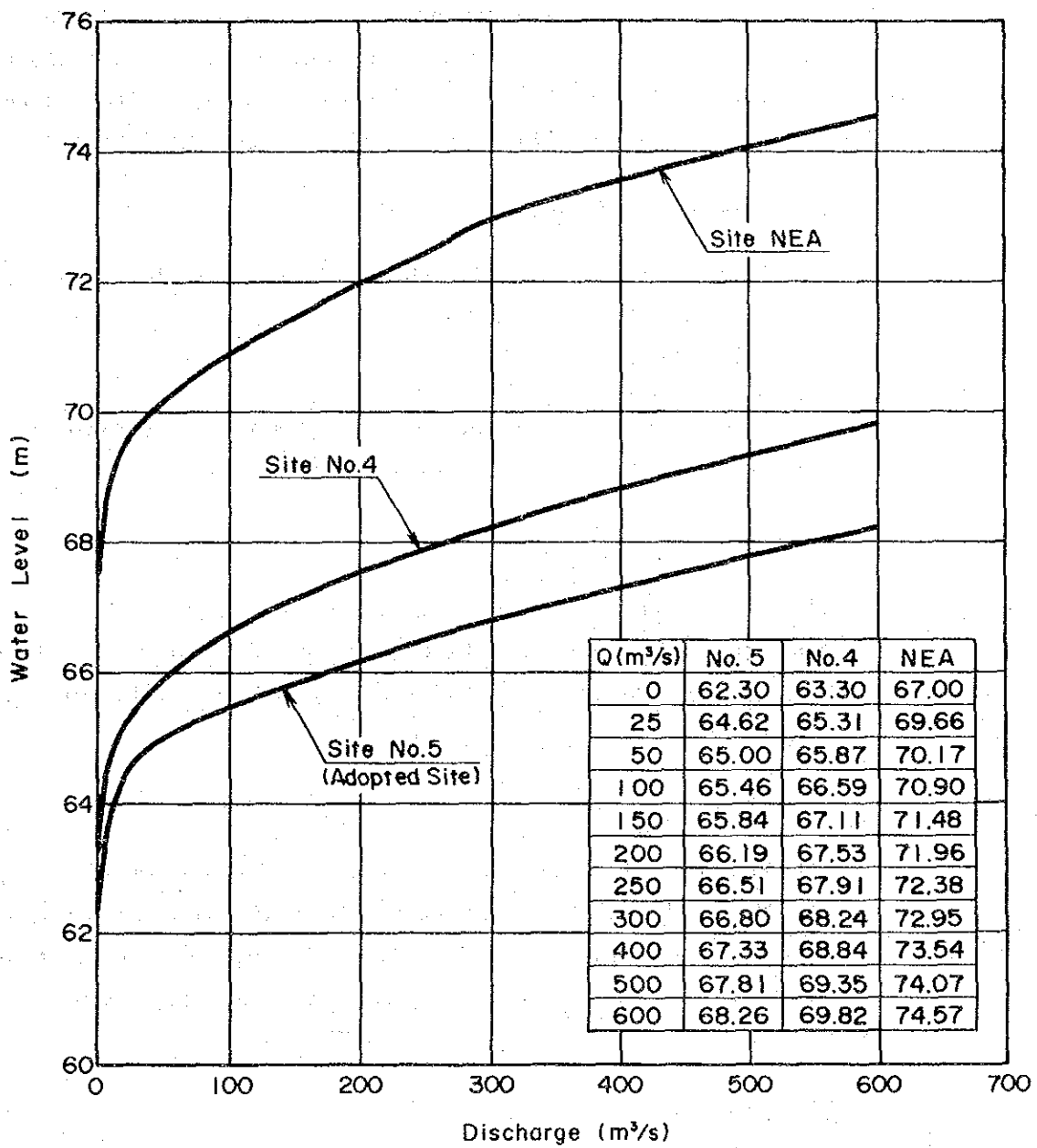


Fig.8-5 Rating Curves of Mae Lama Luang Project